An allosteric model of calmodulin explains differential activation of PP2B and CaMKII

Melanie I. Stefan, Stuart J. Edelstein, and Nicolas Le Novère*

European Molecular Biology Laboratory–European Bioinformatics Institute, Wellcome Trust Genome Campus, Hinxton CB10 1SD, United Kingdom

Communicated by Jean-Pierre Changeux, Institut Pasteur, Paris, France, May 15, 2008 (received for review January 15, 2008)

Calmodulin plays a vital role in mediating bidirectional synaptic plasticity by activating either calcium/calmodulin-dependent protein kinase II (CaMKII) or protein phosphatase 2B (PP2B) at different calcium concentrations. We propose an allosteric model for calmodulin activation, in which binding to calcium facilitates the transition between a low-affinity [tense (*T*)] and a high-affinity [relaxed (*R*)] state. The four calcium-binding sites are assumed to be nonidentical. The model is consistent with previously reported experimental data for calcium binding to calmodulin. It also accounts for known properties of calmodulin that have been difficult to model so far, including the activity of nonsaturated forms of calmodulin (we predict the existence of open conformations in the absence of calcium), an increase in calcium affinity once calmodulin is bound to a target, and the differential activation of CaMKII and PP2B depending on calcium concentration.

allostery | synaptic plasticity | calcium binding | cooperativity | conformational transition

Activity-dependent changes in synaptic strength (1) have long been used as a paradigm to study learning and memory (reviewed in ref. 2). Calcium signaling is a key factor in both long-lasting increases [known as long-term potentiation (LTP)] and long-lasting decreases [long-term depression (LTD)] in synaptic strength. According to a model first proposed by Lisman (3), the coordinated activity of a pair of neurons leads to a large increase in calcium levels in the postsynaptic neuron and an increase in synaptic strength, whereas the activity of only one of the two neurons results in more moderate postsynaptic calcium levels and, consequently, a reduction in synaptic strength. Calcium entering the postsynaptic neuron through NMDA receptors and voltage-operated calcium channels and from the endoplasmic reticulum activates calmodulin. Activated calmodulin may bind to calcium/calmodulin kinase II (CaMKII) and increases its activity (4–6). Active CaMKII enhances the function of AMPA receptor channels by phosphorylating the GluR1 subunit (7). It also mediates an increase of AMPA receptor delivery to the postsynaptic membrane (8). These roles are consistent with reports implicating CaMKII in some forms of learning and memory (9). In contrast, lower amounts of calcium in the postsynaptic neuron will cause calmodulin to activate PP2B, leading to activation of protein phosphatase 1 and a subsequent reduction of CaMKII activity (reviewed in ref. 10). It remains to be explained, however, how calmodulin performs this dual function dependent on calcium levels.

Calmodulin is a ubiquitous regulatory protein that binds four calcium ions (11, 12). It is a single polypeptide chain of 148-aa residues (13) and can adopt two distinct conformations: in the absence of calcium, its EF hands typically adopt an inactive, compact (closed) form (14). When bound to four calcium ions, they are found in an open active form (15).

A variety of models for calmodulin activation and action have been used in the past. Each of these models reflects some properties of calmodulin and is reasonably applicable in contexts in which only these properties are relevant. However, none of these models can satisfactorily account for all of the observed properties of calmodulin such as cooperativity of calcium binding and different affinities for different calcium-binding sites (16), activation of targets by unsaturated calmodulin (17, 18), and increased affinity for calcium upon binding to targets (18–20). We propose an alternative model, based on a biophysical description of the conformational transitions. Originally applied to oligomeric proteins with symmetric identical subunits (21), this approach can also be adapted to a single polypeptide chain with multiple binding sites. The resulting generalized allosteric model of calmodulin can reconcile different properties of calmodulin, including differential activation of PP2B and CaMKII, residual activation of CaMKII at low calcium concentration, differences between the binding sites in terms of calcium affinity, and the existence of active and inactive conformations.

Allosteric Model of Calmodulin. In our model, calmodulin can exist in two different states, the active open [relaxed (*R*)] state and the inactive closed [tense (*T*)] state. Each of these states can bind four calcium ions (Fig. 1). When no calcium is bound, the *T* state prevails, because its free energy is lower than that of the unbound *R* state. Consecutive binding of calcium ions, however, progressively stabilizes the *R* state until the free energy of the *R* state is lower than that of the *T* state, so the *R* state is favored.

The four different binding sites are designated *A*, *B*, *C*, and *D* (*A* and *B* on the N-terminal domain, *C* and *D* on the C-terminal domain, with no sequential order being implied within the domains). Each of the states and each of the reactions is explicitly modeled, with distinct dissociation constants and *R* to *T* transition probabilities for each of the sites (Fig. 2). The constant *L* describes the equilibrium between both states when no calcium ion is bound: $L = [T_0]/[R_0]$. If *L* is very large, most of the protein exists in the tense state in the absence of calcium. If *L* is small (close to one), the *R* state is nearly as populated as the *T* state. The constants c_A, c_B, c_C, and c_D describe the ratio of dissociation constants for the *R* and *T* states for each site: $c_i = K_i^R/K_i^T$. If *c* is one, both *R* and *T* states have the same affinity for calcium. The *c* values also indicate how much the equilibrium between *T* and *R* states changes upon calcium binding: the smaller *c*, the more the equilibrium shifts toward the *R* state.

The formula for fractional occupation of an allosteric protein in the absence of allosteric effectors (21) can be generalized to describe nonequivalent calcium-binding sites. In the case of four binding sites, the generalized expression is:

$$\bar{Y} = 0.25\,\frac{\sum_i \left(\alpha_i \prod_j (1+\alpha_j)\right) + L\,\sum_i \left(c_i\alpha_i \prod_j (1+c_j\alpha_j)\right)}{\prod_i (1+\alpha_i) + L\,\prod_i (1+c_i\alpha_i)}, \quad [1]$$

Author contributions: M.I.S. and N.L. designed research; M.I.S. and N.L. performed research; M.I.S. and S.J.E. analyzed data; and M.I.S., S.J.E., and N.L. wrote the paper.

The authors declare no conflict of interest.

Data deposition: The model reported in this paper has been deposited in the BioModels database, www.ebi.ac.uk/biomodels (accession code MODEL9885984404).

*To whom correspondence should be addressed. E-mail: lenov@ebi.ac.uk.

This article contains supporting information online at www.pnas.org/cgi/content/full/0804672105/DCSupplemental.

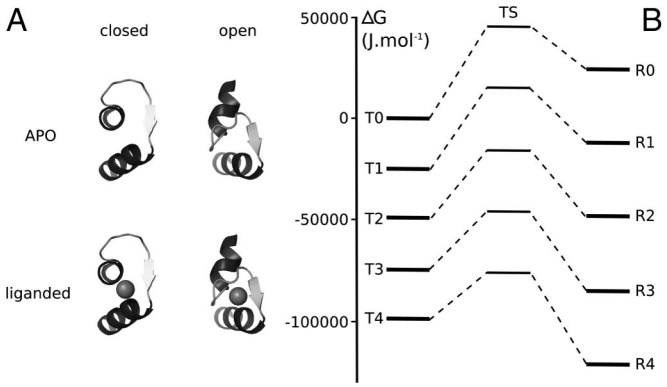

Fig. 1. Thermodynamic model of calmodulin regulation by calcium. (*A*) Representative structures of a calmodulin EF hand modeled in this article. Residues 49–75 are shown. The closed *apo* structure comes from (14) [Protein Data Bank (PDB) ID code: 1CFD]. The closed calcium-liganded structure is inferred from (51) (PDB ID code: 2PQ3), using the position of Zn^{2+}. The open structures come from (52) (PDB ID code: 3CLN). (*B*) Summarized free energy diagram for the different states of calmodulin. Energy levels (in joules per mole) were computed as in ref. 62. Each level of energy represents the average of all of the forms carrying the same number of calcium ions. Free energy differences between *T* state and corresponding *R* state relate to the allosteric isomerization constant. Between corresponding *T* and *R* states, a hypothetical transition state is depicted based on estimates of rate constants. Closed *T* state is shown on the left, open *R* state on the right, and the transition state in the middle.

where $i, j \in \{A, B, C, D\}$, and $j \neq i$. $\alpha_i = [Ca^{2+}]/K_i^R$, where K_i^R denotes the dissociation constant for calcium to site i in the R state.

In a similar way, a general formulation for the fraction of protein in the R state, $\bar{R}$, can be expressed as:

$$\bar{R} = \frac{\prod_i (1 + \alpha_i)}{\prod_i (1 + \alpha_i) + L \prod_i (1 + c_i\alpha_i)}, \qquad [2]$$

where $i \in \{A, B, C, D\}$. The model was further extended to include calmodulin binding to its targets. It was shown that autoinhibitor domains of CaMKII and PP2B bound to the same, open, conformation of calmodulin (22, 23). Therefore, we

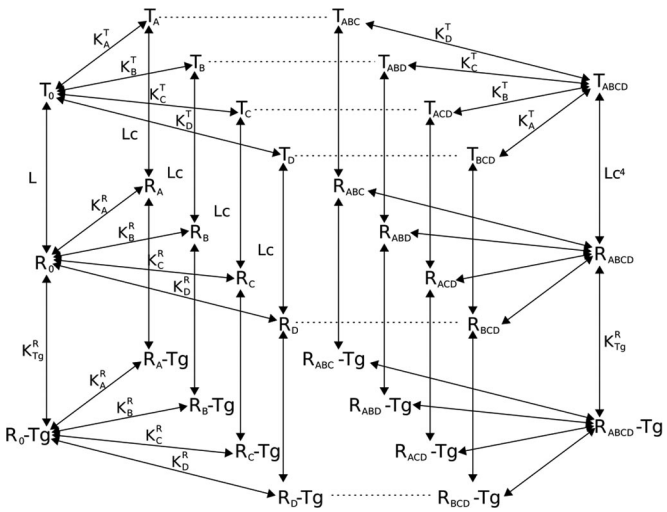

Fig. 2. Scheme of reactions used in the allosteric model of calmodulin. For clarity, only the first and fourth calcium-binding events are depicted in detail. Tg stands for target, which can be either CaMKII or PP2B.

introduced the binding of both CaMKII and PP2B to calmodulin in the R state, independent of the number of bound calcium ions. Upon binding to its targets, the equilibrium of calmodulin shifts toward the R state, and the targets thus act as allosteric activators for calmodulin.

Parameter Determination. The allosteric isomerization constant, L, the microscopic dissociation constants K_i^R for the R state for each binding site, and the ratios of R and T state affinity, c_i, for each site, cannot be directly obtained from experimental literature. Experimental results do allow us, however, to constrain parameter space and obtain reasonable estimates. We used calcium-binding data in the presence and absence of an allosteric activator for mutant and wild-type forms of calmodulin.

We introduced the additional assumption that all four c_i values are identical. This is based on the fact that both R and T states are symmetrical and on the idea that the free energy of transition is spread over the whole molecule.

To obtain an estimate of c and of the isomerization constant L, a reduced model of calmodulin was used. In this simple model, all four calcium-binding sites are equivalent, and one molecule of allosteric activator can bind to each molecule of calmodulin. In this case, the fractional occupation $\bar{Y}$ of an allosteric protein in the presence of an allosteric activator can be described as (24):

$$\bar{Y} = \frac{\alpha(1 + \alpha)^3 + L\left(\frac{1 + \gamma e}{1 + \gamma}\right)c\alpha(1 + c\alpha)^3}{(1 + \alpha)^4 + L\left(\frac{1 + \gamma e}{1 + \gamma}\right)(1 + c\alpha)^4}. \qquad [3]$$

In this equation, $\alpha = [Ca^{2+}]/K_R$, $\gamma = [A]/K_{AR}$, and $e = K_{AR}/K_{AT}$; K_R denotes the dissociation constant for calcium binding to the R state, L the allosteric equilibrium constant, $[A]$ the concentration of allosteric activator, K_{AR} the dissociation constant for binding of the allosteric activator to the R state, and K_{AT} the dissociation constant for binding of the allosteric activator to the T state. The factor $(1 + \gamma e)/(1 + \gamma)$ modulates the apparent isomerization constant as a function of activator concentration: if more target is present, the apparent value of L decreases. Peersen *et al.* (25) have measured calcium binding to calmodulin in the absence and presence of several target proteins, which act as allosteric effectors of calmodulin. By taking the calcium concentration at $\bar{Y} = 1/2$ from four different binding curves (absence of target, presence of skMLCK, PhK5, or CaATPase, respectively) and inserting them into the above equation, we obtained a system of four equations, which depend on L, c, and on e values for skeletal myosin light chain kinase, phosphorylase kinase, and Ca^{2+}-ATPase, respectively. We minimized this system of equations by using the least-square function provided in Scilab (www.scilab.org). To avoid local minima, we ran 10^5 minimizations, each one with different initial values. By this approach we estimated L to be 20,670 and c to be 3.96×10^{-3}. A full list of equations and details about the minimization process are given in supporting information (SI).

To determine the dissociation constants for all four binding sites, we used a similar approach, making use of the general formula for fractional occupancy presented above (Eq. **1**). The formula can be simplified to reflect calmodulin binding to calcium under different experimental constraints. For instance, it can be reduced to the two N-terminal binding sites to describe recombinant versions of calmodulin in which the C-terminal binding sites are ablated. Using the available experimental literature, one thus obtains a system of four equations and corresponding data: the full equation for $\bar{Y}$ (using data from ref. 26), two reduced equations for $\bar{Y}$ with N- or C-terminal binding sites only, respectively (using data from experiments with recombinant calmodulin from ref. 18) and one reduced equation

BIOCHEMISTRY

for $\bar{Y}$ in which only the R state is considered (using data from ref. 25 in the presence of skMLCK, where it can be assumed that calmodulin exists mostly in the R state). There are thus four constraints that can be used to restrict parameter space. We used the calcium concentration at $\bar{Y} = \frac{1}{2}$ and at $\bar{Y} = \frac{1}{4}$ from the experimental literature to obtain eight equations that depend on K_i^R values. The eight equations are listed in SI.

To avoid the problem of local minima, we resorted to systematic sampling of parameter space and generated a script that tested all possible combinations of K_i^R values within a broad range. A detailed description of this can be found in SI. The resulting values are $K_A^R = 8.32 \times 10^{-6}$ M, $K_B^R = 1.66 \times 10^{-8}$ M, $K_C^R = 1.74 \times 10^{-5}$ M, and $K_D^R = 1.45 \times 10^{-8}$ M.

Kinetic Simulations. Although Eq. **1** provides a general formula for calcium saturation in the case of four nonequivalent binding sites in the absence of allosteric effectors, the situation becomes less tractable in the presence of two competing allosteric activators (CaMKII and PP2B, in this case), especially at low calcium concentrations, where initial calcium concentration can differ significantly from free calcium concentration at steady state. Moreover, our intention was to provide an accurate model of calmodulin activation, which can serve as a basis for more complex models of signaling networks within the postsynaptic density (PSD). Both these concerns can be met by formulating the model as a system of reactions for kinetic simulations.

Every reaction was split into a separate forward and backward reaction. The full model comprises 352 reactions: 32 reactions describing calcium binding to the target-free T state, 32 reactions describing the corresponding dissociation events, 64 reactions describing calcium binding to and dissociation from the target-free R state, 32 reactions describing transitions between the R and T states, 32 reactions describing the binding and dissociation of CaMKII, another 32 reactions describing the binding and dissociation of PP2B, and 128 reactions describing calcium binding to and dissociation from CaMKII- or PP2B-bound calmodulin. A complete list of reactions can be found in SI.

The k_{on} for calcium binding was assumed to be the same for all four binding sites and both states, because it can be assumed to be controlled only by calcium and calmodulin diffusion and size (random exploration). Different affinities were represented by different k_{off} values.

Simulations were run by using the parameter-scan facility of the simulator COPASI (27).

Comparison of Calcium-Binding Curve to Experimental Results. Our model reproduces experimental measurements of calmodulin binding to calcium. Fig. 3 compares the outcome of our simulation with results reported by Crouch and Klee (16). [For more figures comparing the simulation outcome with data reported by Peersen *et al.* (25) and Porumb (30), refer to SI.]

Apparent sequential association constants obtained by fitting a version of the Adair equation (43) to our model are listed in Table 1. A comparison to association constants reported in the experimental literature about calmodulin (16, 18, 28–30) shows that our association constants lie within the range of experimentally determined values.

Activity of Various Forms of Nonsaturated Calmodulin. By calculating the equilibrium constant for the transition between R and T states for calmodulin species that are bound to one or more calcium ions, one can see what fraction of calmodulin is active under steady-state conditions.

For instance, the relation between the R and T states for calmodulin with exactly two calcium ions bound is given by $(R_2/T_2 = 1/(Lc^2 \approx 3)$. Similarly, without any calcium bound, there are more than 20,000× more calmodulin molecules in the T than in the R state. With one calcium ion bound, there are still ≈80× more calmodulin molecules in the T than in the R state. The equilibrium shifts toward the R state when two or more calcium ions are bound: with three calcium ions bound, there is ≈800× as much calmodulin in the R state as in the T state, and when fully saturated, there are nearly 200,000 calmodulin molecules in the R state for each calmodulin molecule in the T state. The shift of equilibrium from T to R state with three or more calcium ions bound can also be seen from the free energy diagram (see Fig. 1).

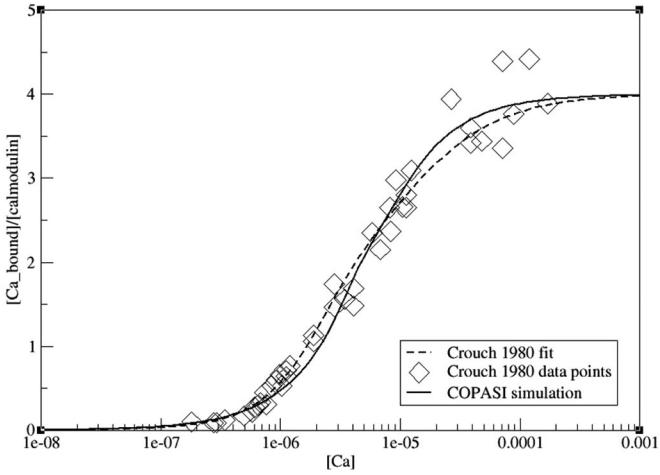

Fig. 3. Comparison between simulation results and experimental results reported by Crouch and Klee (16). Moles of calcium bound per mole of calmodulin are shown as a function of calcium concentration. Diamonds, data points measured by Crouch and Klee (16); dashed line, curve used in Crouch and Klee to fit experimental data points; solid line, steady-state results of simulations at different initial calcium concentrations. Calmodulin concentration used was 2×10^{-7} M.

Altered Affinity for Calcium if Calmodulin Is Bound to a Target. It has been reported (18–20) that the apparent affinity of calmodulin for calcium increases if calmodulin is bound to a target. To reproduce this effect, we simulated calcium binding to 2×10^{-7} M calmodulin at varying calcium concentrations in the absence of target and in the presence of CaMKII. We also performed simulations on two reduced models, representing only the R state or only the T state of calmodulin, respectively. Results are shown in Fig. 4. The fractional occupancy curve illustrates how, with increasing calcium concentration, the calmodulin population shifts from mostly T state to mostly R state, with the corresponding affinities for calcium. The presence of target further

Table 1. Apparent sequential association constants (molar) for our model, and comparison to the models of Crouch and Klee (16), Porumb (30), and to other experimental reports (18, 28–30) and data reviews (28)

	Our model	Crouch and Klee (16)	Porumb (30)	Reported range
K_1	4.7×10^5	3×10^5	2.0×10^5	1.16×10^5*–1.7×10^6*
K_2	3.7×10^5	8.6×10^5	8.9×10^5	1.4×10^5*–8.9×10^5†
K_3	1.5×10^5	1.2×10^5	3.2×10^4	2.86×10^4‡–2.9×10^6*
K_4	3.7×10^4	4.5×10^4	1×10^5	1.7×10^3§–1.12×10^5‡

Constants were obtained by fitting the simulation result with an Adair-type equation (43) as used, for instance, by Crouch and Klee (16) and Porumb (30).
*Ref. 28.
†Ref. 30.
‡Ref. 18.
§Ref. 29.

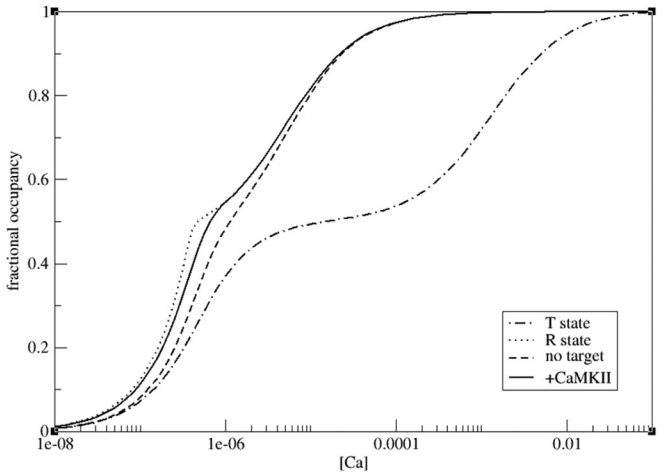

Fig. 4. Increased affinity of calmodulin for calcium in the presence of a target protein. Upper dotted line, *R* state only; lower dotted/dashed line, *T* state only; dashed line, combined *R* and *T* states in the absence of target; solid line, combined *R* and *T* states in the presence of CaMKII. All lines are steady-state results of simulations at different initial calcium concentrations. Calmodulin concentration was 2×10^{-7} M.

stabilizes the *R* state, resulting in the observed increase of affinity.

Differential Activation of CaMKII and PP2B. An intriguing feature of calmodulin is its ability to differentially activate PP2B or CaMKII, depending on calcium input. It is known that PP2B has a much higher affinity for calmodulin (31) than CaMKII (32). However, although PP2B has been detected in PSD fractions (reviewed in ref. 33), CaMKII is far more abundant and, in fact, constitutes a major PSD protein (34, 35). Together with our allosteric model, this information can explain the differential activation of PP2B at low calcium concentrations and of CaMKII at high calcium concentrations.

As Fig. 5 shows, we can reproduce a differential activation of PP2B and CaMKII in our model. At subsaturating calcium concentrations, PP2B becomes preferentially activated due to its high affinity for the *R* state. PP2B binding stabilizes the *R* state and thus increases the apparent affinity of calmodulin for its

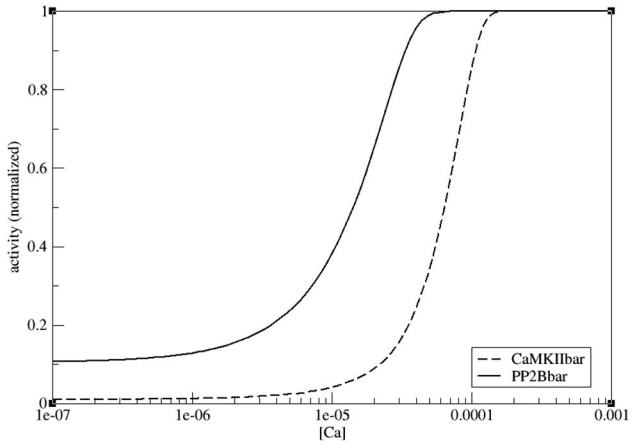

Fig. 5. Differential activation of PP2B and CaMKII at different calcium concentrations. Binding of both PP2B and CaMKII to calmodulin is shown normalized to maximum binding. Steady-state results of simulations at different initial concentrations of calcium are shown. Solid line, PP2B; dashed line, CaMKII. Calmodulin concentration was 3×10^{-5} M (see ref. 36).

targets. At higher calcium concentrations, more calmodulin in the *R* state is available and can bind to CaMKII. Because of the abundance of CaMKII, there is more active CaMKII than PP2B in absolute terms.

Discussion

Induced-Fit Models vs. Thermal Equilibrium Models. Both experimentalists (37) and theoreticians (38) have directly related calmodulin activity to calcium concentration, often by using a Hill function (39). This allows for some calmodulin activity even at low calcium concentrations. Furthermore, together with the facts that calmodulin affinity for PP2B (31) is higher than for CaMKII (32) and that CaMKII concentration in the PSD (40) is higher than PP2B concentration (41), it can explain why PP2B is preferentially activated at lower calcium concentrations. Models of this type do not allow for the possibility that the different binding sites might have different affinities for calcium. Recent experiments on recombinant calmodulin with site-directed mutations, however, suggest that the N-terminal binding sites have different affinities than the C-terminal binding sites (18). Finally, use of a Hill function to compute calmodulin activity as a function of calcium concentration is purely phenomenological and does not provide an explanation for how calcium binding relates to calmodulin activity.

Many investigators measuring calcium binding to calmodulin (16, 18, 28, 42) have used an Adair function (43), or a modified version thereof, to describe calmodulin binding to calcium. This approach allows for different microscopic affinities for the four binding events and thus for detailed models of calcium binding to calmodulin. These models do not, however, explain the transition of calmodulin between closed (''inactive'') and open (''active'') conformations.

Another way to model calmodulin action is by assuming a sequential mechanism, where calmodulin first binds four calcium ions and only then becomes activated (44, 45). These models are useful approximations of how calmodulin activates CaMKII, but they fail to account for important aspects of calmodulin function, all of which can be explained by our model.

A sequential model fails to explain why calmodulin can activate PP2B or CaMKII when bound to less than four calcium ions (17, 18). Some models assume that calmodulin can activate PP2B with two, three, or four calcium ions bound but requires four calcium ions bound to activate CaMKII (49). Although these models are decent phenomenological approximations for modeling the differential activation of CaMKII and PP2B, they do not provide a satisfactory mechanism by which calmodulin with three bound calcium ions activates PP2B, but not CaMKII. By postulating an equilibrium between inactive and active states that is shifted toward the active state by calcium, our model allows for calmodulin activity even when bound to less than four calcium ions. One can see the extent of this by looking at what fraction of subsaturated calmodulin becomes activated. As shown above, ≈75% of calmodulin molecules are active even when only two molecules of calcium are bound. This can explain experiments with mutant calmodulin showing that even when two of the calcium-binding sites are ablated, calmodulin can still activate CaMKII to a certain extent (18). It is also consistent with experimental data showing that conformational transitions exist in *apo* calmodulin (46), and that both *apo* calmodulin and calmodulin bound to only one calcium ion can exist in open and closed states (47). Finally, calmodulin open structures have been found where only one head was populated by calcium (48).

Because purely sequential models do not allow for subsaturated calmodulin binding to its target, they necessarily fail to account for the fact that the affinity of calmodulin for calcium increases once calmodulin is bound to a target (18–20). In our model, subsaturated calmodulin can bind to its targets. The apparent increase for calcium upon binding to targets arises from

the fact that targets act as allosteric activators, drawing the equilibrium toward the high-affinity *R* state.

Note that a simple model based on thermal equilibrium has been proposed before (50), although based on sequential bindings of calcium. Furthermore, the author did not try to estimate parameters using experimental information or to validate the model.

Model Characteristics. The association constants we determined from the simulation result by fitting it with an Adair-type equation (43) are the observable sequential association constants for the first, second, third, and fourth binding events. It is important to note, however, that our model does not assume a fixed order for calcium binding to the different binding sites. Rather, because the first calcium ion can bind to any one of four binding sites in either state, K_1 is a combination of the microscopic K_i^R and K_i^T values for each of the sites in each of the states. The apparent sequential dissociation constants used in our model follow an Adair-type (43) framework as used, for instance, by Crouch and Klee (16) and Porumb (30). They are, in principle, Adair constants, except for a slight difference in nomenclature: K_2 according to Adair (43) corresponds to $K_1 \times K_2$ according to Crouch and Klee (16) and Porumb (30), and so on.

It is important to note that the conformation of calmodulin which we call the *T* state is not necessarily exactly identical to the reported *apo* structure (14) of calmodulin. Rather, the *T* state represents a collection of structures that may differ somewhat in the conformation of the calcium-binding sites, but whose overall structure resembles that of *apo* calmodulin. The existence of an ion-bound form that resembles the *apo* conformation has recently been established (51). Likewise, the *R* state is a collection of structures that resemble the reported open structure of active calmodulin (52, 53). Asymmetric forms of calmodulin with one lobe in an open state and one head in a closed state have been reported in the presence of some targets (54). However, the binding mechanism of these targets differs from that of CaMKII and PP2B, where both lobes bind to the target.

Lisman Hypothesis. The model proposed here explains how different amounts of calcium can trigger the activation of PP2B or CaMKII and thus provides support for the Lisman hypothesis (3) on a molecular level. The question of how different frequencies of calcium signals lead to differential activation of PP2B or CaMKII is not addressed in the model. It has been suggested, however, that, at least under some conditions, high frequencies of calcium input result in high local concentrations of calcium, whereas low calcium frequencies result in moderate local calcium concentrations in the spine (44, 55, 56). In addition, calcium frequency has a direct impact on CaMKII, because of the requirement for two adjacent subunits to be active for autophosphorylation at threonine residue 286, which confers sustained activity (57–59). Other factors the model does not account for include variations in the subcellular localization of PP2B (reviewed in ref. 60) and CaMKII (61) and the inhibitory effect of PP2B on CaMKII (reviewed in ref. 10). The latter effect, if included, would increase the window of calcium concentrations at which PP2B is preferably activated, enhancing the distinction between PP2B and CaMKII activation. We believe, however, that our model provides a valid and useful biophysical basis on which to develop further models of synaptic plasticity mechanisms.

Note added in proof (64). Experimental support for our equilibrium model of calmodulin function has been recently published by Gsponer *et al*.

ACKNOWLEDGMENTS. We thank Julia Shifman (Hebrew University of Jerusalem) for sharing raw data on calcium binding to calmodulin in the presence and absence of CaMKII. We also thank Laurence Calzone, Stephen Martin, and Annalisa Pastore for helpful comments on the manuscript. S.J.E. was supported by an International Short Visit Fellowship from the Royal Society.

1. Bliss TV, Lomo T (1973) Long-lasting potentiation of synaptic transmission in the dentate area of the anaesthetized rabbit following stimulation of the perforant path. *J Physiol* 232:331–356.
2. Martin SJ, Grimwood PD, Morris RG (2000) Synaptic plasticity and memory: An evaluation of the hypothesis. *Annu Rev Neurosci* 23:649–711.
3. Lisman J (1989) A mechanism for the Hebb and the anti-Hebb processes underlying learning and memory. *Proc Natl Acad Sci USA* 86:9574–9578.
4. Schulman H, Greengard P (1978) Stimulation of brain membrane protein phosphorylation by calcium and an endogenous heat-stable protein. *Nature* 271:478–479.
5. Schulman H, Greengard P (1978) Ca2+-dependent protein phosphorylation system in membranes from various tissues, and its activation by ''calcium-dependent regulator.'' *Proc Natl Acad Sci USA* 75:5432–5436.
6. Lisman J, Schulman H, Cline H (2002) The molecular basis of CaMKII function in synaptic and behavioural memory. *Nat Rev Neurosci* 3:175–190.
7. Lee HK, Barbarosie M, Kameyama K, Bear MF, Huganir RL (2000) Regulation of distinct AMPA receptor phosphorylation sites during bidirectional synaptic plasticity. *Nature* 405:955–959.
8. Hayashi Y, *et al.* (2000) Driving AMPA receptors into synapses by LTP and CaMKII: Requirement for GluR1 and PDZ domain interaction. *Science* 287:2262–2267.
9. Silva AJ, Paylor R, Wehner JM, Tonegawa S (1992) Impaired spatial learning in alpha-calcium-calmodulin kinase II mutant mice. *Science* 257:206–211.
10. Groth RD, Dunbar RL, Mermelstein PG (2003) Calcineurin regulation of neuronal plasticity. *Biochem Biophys Res Commun* 311:1159–1171.
11. Lin YM, Liu YP, Cheung WY (1974) Cyclic 3′:5′-nucleotide phosphodiesterase. Purification, characterization, and active form of the protein activator from bovine brain. *J Biol Chem* 249:4943–4954.
12. Xia Z, Storm DR (2005) The role of calmodulin as a signal integrator for synaptic plasticity. *Nat Rev Neurosci* 6:267–276.
13. Watterson DM, Sharief F, Vanaman TC (1980) The complete amino acid sequence of the Ca2+-dependent modulator protein (calmodulin) of bovine brain. *J Biol Chem* 255:962–975.
14. Kuboniwa H, *et al.* (1995) Solution structure of calcium-free calmodulin. *Nat Struct Biol* 2:768–776.
15. Babu YS, *et al.* (1985) Three-dimensional structure of calmodulin. *Nature* 315:37–40.
16. Crouch TH, Klee CB (1980) Positive cooperative binding of calcium to bovine brain calmodulin. *Biochemistry* 19:3692–3698.
17. Kincaid RL, Vaughan M (1986) Direct comparison of Ca2+ requirements for calmodulin interaction with and activation of protein phosphatase. *Proc Natl Acad Sci USA* 83:1193–1197.
18. Shifman JM, Choi MH, Mihalas S, Mayo SL, Kennedy MB (2006) Ca2+/calmodulin-dependent protein kinase II (CaMKII) is activated by calmodulin with two bound calciums. *Proc Natl Acad Sci USA* 103:13968–13973.
19. Burger D, Stein EA, Cox JA (1983) Free energy coupling in the interactions between Ca2+, calmodulin, and phosphorylase kinase. *J Biol Chem* 258:14733–14739.
20. Olwin BB, Edelman AM, Krebs EG, Storm DR (1984) Quantitation of energy coupling between Ca2+, calmodulin, skeletal muscle myosin light chain kinase, and kinase substrates. *J Biol Chem* 259:10949–10955.
21. Monod J, Wyman J, Changeux JP (1965) On the nature of allosteric transitions: A plausible model. *J Mol Biol* 12:88–118.
22. Meador WE, Means AR, Quiocho FA (1992) Target enzyme recognition by calmodulin: 2.4 A structure of a calmodulin-peptide complex. *Science* 257:1251–1255.
23. Ye Q, Li X, Wong A, Wei Q, Jia Z (2006) Structure of calmodulin bound to a calcineurin peptide: A new way of making an old binding mode. *Biochemistry* 45:738–745.
24. Rubin MM, Changeux JP (1966) On the nature of allosteric transitions: Implications of non-exclusive ligand binding. *J Mol Biol* 21:265–274.
25. Peersen OB, Madsen TS, Falke JJ (1997) Intermolecular tuning of calmodulin by target peptides and proteins: Differential effects on Ca2+ binding and implications for kinase activation. *Protein Sci* 6:794–807.
26. Bayley PM, Findlay WA, Martin SR (1996) Target recognition by calmodulin: Dissecting the kinetics and affinity of interaction using short peptide sequences. *Protein Sci* 5:1215–1228.
27. Hoops S, *et al.* (2006) COPASI–a COmplex PAthway SImulator. *Bioinformatics* 22:3067–3074.
28. Burger D, Cox JA, Comte M, Stein EA Sequential (1984) Conformational changes in calmodulin upon binding of calcium. *Biochemistry* 23:1966–1971.
29. Haiech J, Klee CB, Demaille JG (1981) Effects of cations on affinity of calmodulin for calcium: Ordered binding of calcium ions allows the specific activation of calmodulin-stimulated enzymes. *Biochemistry* 20:3890–3897.
30. Porumb T (1994) Determination of calcium-binding constants by flow dialysis. *Anal Biochem* 220:227–237.
31. Quintana AR, Wang D, Forbes JE, Waxham MN (2005) Kinetics of calmodulin binding to calcineurin. *Biochem Biophys Res Commun* 334:674–680.
32. Tzortzopoulos A, Török K (2004) Mechanism of the T286A-mutant alphaCaMKII interactions with Ca2+/calmodulin and ATP. *Biochemistry* 43:6404–6414.
33. Collins MO, *et al.* (2006) Molecular characterization and comparison of the components and multiprotein complexes in the postsynaptic proteome. *J Neurochem* 97:16–23.
34. Chen X, *et al.* (2005) Mass of the postsynaptic density and enumeration of three key molecules. *Proc Natl Acad Sci USA* 102:11551–11556.

35. Cheng D, *et al.* (2006) Relative and absolute quantification of postsynaptic density proteome isolated from rat forebrain and cerebellum. *Mol Cell Proteomics* 5:1158–1170.
36. Kakiuchi S, *et al.* (1982) Quantitative determinations of calmodulin in the supernatant and particulate fractions of mammalian tissues. *J Biochem* 92:1041–1048.
37. Pifl C, *et al.* (1984) Calmodulin X (Ca2+)4 is the active calmodulin-calcium species activating the calcium-, calmodulin-dependent protein kinase of cardiac sarcoplasmic reticulum in the regulation of the calcium pump. *Biochim Biophys Acta* 773:197–206.
38. d'Alcantara P, Schiffmann S, Swillens S (2003) Bidirectional synaptic plasticity as a consequence of interdependent Ca2+-controlled phosphorylation and dephosphorylation pathways. *Eur J Neurosci* 17:2521–2528.
39. Hill AV (1913) The combinations of haemoglobin with oxygen and with carbon monoxide. *Biochem J* 5:471–480.
40. Petersen JD, *et al.* (2003) Distribution of postsynaptic density (PSD)-95 and Ca2+/calmodulin-dependent protein kinase II at the PSD. *J Neurosci* 23:11270–11278.
41. Goto S, Matsukado Y, Mihara Y, Inoue N, Miyamoto E (1986) The distribution of calcineurin in rat brain by light and electron microscopic immunohistochemistry and enzyme-immunoassay. *Brain Res* 397:161–172.
42. Mirzoeva S, *et al.* (1999) Analysis of the functional coupling between calmodulin's calcium binding and peptide recognition properties. *Biochemistry* 38:3936–3947.
43. Adair GS (1925) The hemoglobin system. *J Biol Chem* 63:529–545.
44. Franks KM, Bartol TM, Sejnowski TJ (2001) An M cell model of calcium dynamics and frequency-dependence of calmodulin activation in dendritic spines. *Neurocomputing* 38–40:9–16.
45. Naoki H, Sakamira Y, Ishii S (2005) Local signaling with molecular diffusion as a decoder of Ca2+ signals in synaptic plasticity. *Mol Syst Biol* 1:2005.0027.
46. Tjandra N, Kuboniwa H, Ren H, Bax A (1995) Rotational dynamics of calcium-free calmodulin studied by 15N-NMR relaxation measurements. *Eur J Biochem* 230:1014–1024.
47. Malmendal A, Evenäs J, Forsén S, Akke M (1999) Structural dynamics in the C-terminal domain of calmodulin at low calcium levels. *J Mol Biol* 293:883–899.
48. Schumacher MA, Rivard AF, Bächinger HP, Adelman JP (2001) Structure of the gating domain of a Ca2+-activated K+ channel complexed with Ca2+/calmodulin. *Nature* 410:1120–1124.
49. Bhalla US, Iyengar R (1999) Emergent properties of networks of biological signaling pathways. *Science* 283:381–387.
50. Czerlinski GH (1984) Allosteric competition in calmodulin. *Physiol Chem Phys Med NMR* 16:437–447.
51. Warren JT, Guo Q, Tang W-J (2007) A 1.3-A structure of zinc-bound N-terminal domain of calmodulin elucidates potential early ion-binding step. *J Mol Biol* 374:517–527.
52. Babu YS, Bugg CE, Cook WJ (1988) Structure of calmodulin refined at 2.2 A resolution. *J Mol Biol* 204:191–204.
53. Fallon JL, Quiocho FA (2003) A closed compact structure of native Ca(2+)-calmodulin. *Structure* 11:1303–1307.
54. Drum CL, *et al.* (2002) Structural basis for the activation of anthrax adenylyl cyclase exotoxin by calmodulin. *Nature* 415:396–402.
55. Gamble E, Koch C (1987) The dynamics of free calcium in dendritic spines in response to repetitive synaptic input. *Science* 236:1311–1315.
56. Bhalla US (2002) Biochemical signaling networks decode temporal patterns of synaptic input. *J Comput Neurosci* 13:49–62.
57. Dosemeci A, Albers RW (1996) A mechanism for synaptic frequency detection through autophosphorylation of CaM kinase II. *Biophys J* 70:2493–2501.
58. De Koninck P, Schulman H (1998) Sensitivity of CaM kinase II to the frequency of Ca2+ oscillations. *Science* 279:227–230.
59. Dupont G, Houart G, De Koninck P (2003) Sensitivity of CaM kinase II to the frequency of Ca2+ oscillations: A simple model. *Cell Calcium* 34:485–497.
60. Colbran RJ (2004) Protein phosphatases and calcium/calmodulin-dependent protein kinase II-dependent synaptic plasticity. *J Neurosci* 24:8404–8409.
61. Bayer KU, *et al.* (2006) Transition from reversible to persistent binding of CaMKII to postsynaptic sites and NR2B. *J Neurosci* 26:1164–1174.
62. Edelstein SJ, Schaad O, Henry E, Bertrand D, Changeux JP (1996) A kinetic mechanism for nicotinic acetylcholine receptors based on multiple allosteric transitions. *Biol Cybernet* 75:361–379.
63. Keller CH, Olwin BB, LaPorte DC, Storm DR (1982) Determination of the free-energy coupling for binding of calcium ions and troponin I to calmodulin. *Biochemistry* 21:156–162.
64. Gsponer J, *et al*. (2008) A coupled equilibrium shift mechanism in calmodulin-mediated signal transduction. *Structure* (*London*) 16:736–746.

BMC Systems Biology

BioMed Central

Research article

Computing phenomenologic Adair-Klotz constants from microscopic MWC parameters

Melanie I Stefan, Stuart J Edelstein and Nicolas Le Novère*

Address: Computational Neurobiology Group, EMBL-EBI, Wellcome-Trust Genome Campus, Hinxton, CB10 1SD, UK

Email: Melanie I Stefan - mstefan@ebi.ac.uk; Stuart J Edelstein - stuarte@ebi.ac.uk; Nicolas Le Novère* - lenov@ebi.ac.uk

* Corresponding author

Published: 14 July 2009

BMC Systems Biology 2009, **3**:68 doi:10.1186/1752-0509-3-68

Received: 25 September 2008

Accepted: 14 July 2009

This article is available from: http://www.biomedcentral.com/1752-0509/3/68

Abstract

Background: Modellers using the MWC allosteric framework have often found it difficult to validate their models. Indeed many experiments are not conducted with the notion of alternative conformations in mind and therefore do not (or cannot) measure relevant microscopic constant and parameters. Instead, experimentalists widely use the Adair-Klotz approach in order to describe their experimental data.

Results: We propose a way of computing apparent Adair-Klotz constants from microscopic association constants and allosteric parameters of a generalised concerted model with two different states (*R* and *T*), with an arbitrary number of non-equivalent ligand binding sites. We apply this framework to compute Adair-Klotz constants from existing models of calmodulin and hemoglobin, two extreme cases of the general framework.

Conclusion: The validation of computational models requires methods to relate model parameters to experimentally observable quantities. We provide such a method for comparing generalised MWC allosteric models to experimentally determined Adair-Klotz constants.

Background

Quantitative descriptions of biological processes are one of the main activities in Life Science research, whether in physiology, biochemistry or molecular and cellular biology. They offer a way of characterising biological systems, measuring subtle effects of perturbations, discriminating between alternative hypotheses, making and testing predictions, and following changes over time. There can be many different ways to describe the same biological process. Phenomenological descriptions provide a way of relating input and outcome of a given process, without requiring a detailed knowledge about the nature of the process or possible intermediate steps. Since they provide a direct link between input and output, they can be easily applied to experimental results. On the other hand, Systems Biology favours more mechanistic representations, that aim at exploring how exactly behaviours of systems emerge from intrinsic properties and interactions of elements at a lower level. Using the former descriptions to build and validate the latter representations may prove a challenge in some cases.

Several types of descriptions may co-exist for a given biological problem. One of these problems is the binding of ligand to a protein with several binding sites, and the apparent cooperativity observed in this context, for which various frameworks have been developed throughout the XXth century [1].

Drawing on observations of oxygen binding to hemoglobin, Hill [2] suggested the following formula for the fractional occupancy $\bar{Y}$ of a protein with several ligand binding sites:

$$\bar{Y} = \frac{K[X]^n H}{1+K[X]^n H} \quad (1)$$

where K denotes an apparent association constant, $[X]$ denotes ligand concentration, and n_H the "Hill coefficient", intended to be a measure of cooperativity.

Adair [3] and Klotz [4] (reviewed in [5]) further explored the notion of cooperative binding. According to their framework, cooperativity was no longer fixed, but dependent on saturation: There were different binding constants describing binding of the first ligand, the second, the third, etc. It is worth noting that these constants do not relate to individual binding sites. They describe *how many* binding sites are occupied, rather than *which ones*. This framework is often used by experimentalists to describe measurements of ligand binding in terms of sequential apparent binding constants. According to this framework, the fractional occupancy of a protein is given by the following equation [4]:

$$\bar{Y} = \frac{1}{n}\frac{K_1[X]+2K_1K_2[X]^2+\ldots+n(K_1K_2\ldots K_n)[X]^n}{1+K_1[X]+K_1K_2[X]^2+\ldots+(K_1K_2\ldots K_n)[X]^n} \quad (2)$$

Where n denotes the number of binding sites and K_i the i^{th} apparent association constant

The Monod-Wyman-Changeux (MWC) model for concerted allosteric transitions [6] went a step further by exploring cooperativity based on three-dimensional conformations. It was originally formulated for oligomeric proteins with symmetric, identical subunits, each of which has one ligand binding site. According to this framework, two (or more) interconvertible conformational states of an allosteric protein coexist in a thermal equilibrium. The ratio between the two states (often termed "*T*" for "tense", and "*R*" for "relaxed") is regulated by the binding of ligands that have different affnities for each of the states. For instance, in the absence of a ligand, the *T* state prevails, but as more ligand molecules bind, the *R* state (which has higher affnity for the ligand) becomes the energetically favoured conformation. The constant *L* describes the equilibrium between both states when no ligand molecule is bound: $L = [T_0]/[R_0]$. If *L* is very large, most of the protein exists in the tense state in the absence of ligand. If *L* is small (close to one), the *R* state is nearly as populated as the *T* state. The constant *c* describes the ratio of association constants for the *T* and *R* states for each site: $c = K^T/K^R$ (note that MWC equations are most often expressed with dissociation constants. However, we will use association constant throughout this paper for the sake of consistency with Hill and Adair-Klotz schemes). If $c = 1$, both *R* and *T* states have the same ligand affnity. The *c* value also indicates how much the equilibrium between *T* and *R* states changes upon ligand binding: the smaller *c*, the more the equilibrium shifts towards the *R* state. According to the MWC model, fractional occupancy is described by:

$$\bar{Y} = \frac{[X]K^R(1+[X]K^R)^{n-1}+Lc[X]K^R(1+c[X]K^R)^{n-1}}{(1+[X]K^R)^n+L(1+c[X]K^R)^n} \quad (3)$$

where $[X]$ denotes ligand concentration, and with K^R, *L* and *c* as described in the paragraph above. In this paper, we first propose a generalised MWC framework that can be applied to proteins whose ligand binding sites have different affnities. We then develop a set of equations that uses the parameters of such a generalised MWC model to compute apparent association constants according to the Adair-Klotz model. We show how these can be used in order to compare model results with experimental data using two examples which constitute extreme cases of the general framework, calmodulin and hemoglobin.

Results

Generalisation of the MWC model

The MWC model can be adapted to describe a protein (whether oligomeric or monomeric) with several ligand binding sites possessing different affinities. In that case, microscopic association constants are termed K_i^T and K_i^R, and their ratio is denoted by c_i for the i^{th} binding site.

In this case, the fractional occupancy is described as follows:

$$\bar{Y} = \frac{1}{n}\frac{\Sigma_i\left([X]K_i^R\Pi_{j\neq i}(1+[X]K_j^R)\right)+L\Sigma_i\left(c_i[X]K_i^R\Pi_{j\neq i}(1+c_j[X]K_j^R)\right)}{\Pi_i(1+[X]K_i^R)+L\Pi_i(1+c_i[X]K_i^R)} \quad (4)$$

where $1 \leq i, j \leq n$, $c_i = \frac{K_i^T}{K_i^R}$ and *L* and $[X]$ as described above.

If not all binding sites are different, but m_i binding sites have the same affinity K_i^R, identical binding sites can be grouped and the above equation written as:

$$\bar{Y} = \frac{1}{n}\left(\frac{\Sigma_i \left(m_i [X] K_i^R (1+[X]K_i^R)^{m_i-1} \prod_{j\neq i}(1+[X]K_j^R)^{m_j} \right)}{\prod_i (1+[X]K_i^R)^{m_i} + L\prod_i (1+c_i[X]K_i^R)^{m_i}} + \right.$$
$$\left. + \frac{L\Sigma_i \left(m_i c_i [X] K_i^R (1+c_i[X]K_i^R)^{m_i-1} \prod_{j\neq i}(1+c_j[X]K_j^R)^{m_j} \right)}{\prod_i (1+[X]K_i^R)^{m_i} + L\prod_i (1+c_i[X]K_i^R)^{m_i}} \right) \quad (5)$$

where $1 \leq i, j \leq k$, m_i denotes the number of binding sites with affnity K_i^R (note that $\Sigma_i m_i = n$), and L, c_i and $[X]$ as described above.

Similarly, it is possible to develop generalisations of the equation for fractional conformational change ($\bar{R}$). In the case of a protein with n different ligand binding sites, the corresponding expression is:

$$\bar{R} = \frac{\prod_i (1+[X]K_i^R)}{\prod_i (1+[X]K_i^R) + L\prod_i (1+c_i[X]K_i^R)} \quad (6)$$

When all K_i^R and all c_i are equal, this corresponds to the original MWC equation [6].

Again, when binding sites are pooled into groups of m_i binding sites that have the same affnity K_i^R (where $\Sigma_i m_i = n$), then $\bar{R}$ can be written as follows:

$$\bar{R} = \frac{\prod_i (1+[X]K_i^R)^{m_i}}{\prod_i (1+[X]K_i^R)^{m_i} + L\prod_i (1+c_i[X]K_i^R)^{m_i}} \quad (7)$$

In order to compare the numerical outcomes of their models with experimental results, modellers using either the original or the generalised MWC framework need a way of converting microscopic MWC constants into observed Adair-Klotz constants. Here, we derive equations that can be used to compute Adair-Klotz constants and apply them to two special cases of the generalised MWC model presented here.

Obtaining Adair-Klotz constants from microscopic association constants for a protein with four non-equivalent binding sites

Consider a protein P with four binding sites for ligand X. The first apparent association constant, K_1 is defined as follows:

$$K_1 = \frac{[P_1]}{[P_0][X]}$$

where $[P_0]$ denotes the concentration of unbound protein, $[P_1]$ the concentration of protein with exactly one ligand molecule bound and $[X]$ the concentration of ligand. Since P is an allosteric protein, it can exist in two different conformations: The high-affinity R conformation and the low-affinity T conformation. If we denote by $[R_i]$ the concentration of protein in the R state bound to i ligand molecules (and analogous for $[T_i]$), we can re-write the above expression to

$$K_1 = \frac{[R_1]+[T_1]}{([R_0]+[T_0])[X]}$$

Since we treat the four binding sites as non-equivalent, we have to discriminate between them. The first ligand molecule bound to the protein in the R state can bind to either site A, B, C, or D. If R_A denotes the concentration of protein in the R state bound to exactly one ligand molecule at site A (and analogous for sites B, C, and D, and for the T state), the above equation becomes:

$$K_1 = \frac{([R_A]+[R_B]+[R_C]+[R_D])+([T_A]+[T_B]+[T_C]+[T_D]}{([R_0]+[T_0])[X]}$$

The balance between unbound protein in the T and R states is given by the allosteric isomerisation constant, L ($L = \frac{[T_0]}{[R_0]}$). We can now use this relationship and derive an equation that links the apparent first association constant K_1 to the microscopic association constants (K_A^R for site A in the R state, and analogous for the other binding sites, and the T state):

$$K_1 = \frac{([R_0][X]K_A^R+[R_0][X]K_B^R+[R_0][X]K_C^R+[R_0][X]K_D^R)+([T_0][X]K_A^T+[T_0][X]K_B^T+[T_0][X]K_C^T+[T_0][X]K_D^T)}{([R_0]+[T_0])[X]}$$

Substituting for $[T_0]$ and simplifying, we obtain

$$K_1 = \frac{K_A^R+K_B^R+K_C^R+K_D^R+L(K_A^T+K_B^T+K_C^T+K_D^T)}{1+L} \quad (8)$$

In a similar manner we can consider the second association constant, K_2

$$K_2 = \frac{[P_2]}{[P_1][X]}$$

Again, distinguishing between the R and T states and between the four different binding sites, we obtain:

$$K_2 = \frac{[R_{AB}]+[R_{AC}]+[R_{AD}]+[R_{BC}]+[R_{BD}]+[R_{CD}]+[T_{AB}]+[T_{AC}]+[T_{AD}]+[T_{BC}]+[T_{BD}]+[T_{CD}]}{([R_A]+[R_B]+[R_C]+[R_D]+[T_A]+[T_B]+[T_C]+[T_D])[X]}$$

This reduces to:

$$K_2 = \frac{K_A^R K_B^R + K_A^R K_C^R + K_A^R K_D^R + K_B^R K_C^R + K_B^R K_D^R + K_C^R K_D^R + L(K_A^T K_B^T + K_A^T K_C^T + K_A^T K_D^T + K_B^T K_C^T + K_B^T K_D^T + K_C^T K_D^T)}{K_A^R + K_B^R + K_C^R + K_D^R + L(K_A^T + K_B^T + K_C^T + K_D^T)} \quad (9)$$

We can apply the same reasoning to the third ligand binding event:

$$K_3 = \frac{[P_3]}{[P_2][X]}$$

which eventually gives:

$$K_3 = \frac{K_A^R K_B^R K_C^R + K_A^R K_B^R K_D^R + K_A^R K_C^R K_D^R + K_B^R K_C^R K_D^R + L(K_A^T K_B^T K_C^T + K_A^T K_B^T K_D^T + K_A^T K_C^T K_D^T + K_B^T K_C^T K_D^T)}{K_A^R K_B^R + K_A^R K_C^R + K_A^R K_D^R + K_B^R K_C^R + K_B^R K_D^R + K_C^R K_D^R + L(K_A^T K_B^T + K_A^T K_C^T + K_A^T K_D^T + K_B^T K_C^T + K_B^T K_D^T + K_C^T K_D^T)} \quad (10)$$

And, similarly for K_4:

$$K_4 = \frac{[P_4]}{[P_3][X]}$$

$$K_4 = \frac{K_A^R K_B^R K_C^R K_D^R + L K_A^T K_B^T K_C^T K_D^T}{K_A^R K_B^R K_C^R + K_A^R K_B^R K_D^R + K_A^R K_C^R K_D^R + K_B^R K_C^R K_D^R + L(K_A^T K_B^T K_C^T + K_A^T K_B^T K_D^T + K_A^T K_C^T K_D^T + K_B^T K_C^T K_D^T)} \quad (11)$$

Note that in the case of four identical binding sites, $K_A^R = K_B^R = K_C^R = K_D^R =: K^R$ and $K_A^T = K_B^T = K_C^T = K_D^T =: K^T$, and the above expressions reduce to conversion equations for identical binding sites reported by Edelstein [7].

Obtaining the i^th^ *Adair-Klotz constants from microscopic association constants for a protein with* n *non-equivalent binding sites*

In general, for a protein with n ligand binding sites, we can express the apparent association constant for the i^{th} binding event by computing the ratio between the concentrations of end products and initial reactants. The equation for the i^{th} apparent association constant thus reads as follows:

$$K_i^n = \frac{[P_i]}{[P_{i-1}][X]}$$

As above, both $[P_{i-1}]$ and $[P_i]$ are sums of protein populations in two different states and with ligand molecules bound to combinations of different binding sites. We can again distinguish between R and T state, which yields:

$$K_i^n = \frac{[R_i]+[T_i]}{([R_{i-1}]+[T_{i-1}])[X]}$$

If we now assume that the n ligand binding sites are, in general, non-equivalent, we must account for the fact that R_i is a collection of protein molecules in the R state with all possible combinations of i out of n ligand binding sites occupied. In other words:

$$R_i = \sum_{j_1<j_2<\cdots<j_i,\ \text{all } j\in\{1,\ldots,n\}} R_{j_1 j_2 \ldots j_i} \quad (12)$$

Expressing every $R_{j1j2\ldots ji}$ in terms of $[R_0]$, $[X]$ and the microscopic association constants, we can write R_i in the following way:

$$[R_i] = [R_0][X]^i \sum_{j_1<j_2<\cdots<j_i,\ \text{all } j\in\{1,\ldots,n\}} K_{j_1}^R K_{j_2}^R \ldots K_{j_i}^R \quad (13)$$

Introducing the following abbreviations

$$S_i^{nR} := \sum_{j_1<j_2<\cdots<j_i,\ \text{all } j\in\{1,\ldots,n\}} K_{j_1}^R K_{j_2}^R \ldots K_{j_i}^R \quad (14)$$

$$S_i^{nT} := \sum_{j_1<j_2<\cdots<j_i,\ \text{all } j\in\{1,\ldots,n\}} K_{j_1}^T K_{j_2}^T \ldots K_{j_i}^T \quad (15)$$

we can obtain the expression for K_i^n

$$K_i^n = \frac{[R_0][X]^i S_i^{nR} + [T_0][X]^i S_i^{nT}}{([R_0][X]^{i-1} S_{i-1}^{nR} + [T_0][X]^{i-1} S_{i-1}^{nT})[X]}$$

Now, again, we can use the relationship $[T_0] = L\,[R_0]$ and eliminate $[X]^i$ and $[R_0]$ and obtain:

$$K_i^n = \frac{S_i^{nR} + L S_i^{nT}}{S_{i-1}^{nR} + L S_{i-1}^{nT}} \quad (16)$$

with S_i^{nR} and S_i^{nT} as defined above.

If the binding sites can be classed into k sub-groups that have the same affinity (m_1 binding sites with affinity K_1^R m_2 binding sites with affinity K_2^R, etc.), the expression for S_i^{nR} can be written as follows:

$$S_i^{nR} := \sum_{0\le e_j\le m_j, e_1+\ldots+e_k=i} \binom{m_1}{e_1} \left(K_1^R\right)^{e_1} \cdots \binom{m_2}{e_k} \left(K_k^R\right)^{e_k} \quad (17)$$

In the next section, we will consider two proteins with four binding sites each, which constitute extreme cases: In the case of calmodulin, all binding sites are different, so

the protein can be seen as having four sub-groups of binding sites containing one binding site each ($m_1 = m_2 = m_3 = m_4 = 1$). In the case of hemoglobin, all binding sites are equivalent, so there is only one sub-group of binding sites containing four elements.

Allosteric model of calmodulin

To illustrate the practical relevance of these conversion equations we applied them to a previously proposed MWC model of calmodulin [8]. According to this model, calmodulin can exist in two different states, *R* (that corresponds to the open state, stabilised by binding of calcium) and *T* (that correspond to the closed, often mistakenly called "apo", state). Each of these states can bind four calcium ions. The four different binding sites were designated *A*, *B*, *C*, and *D* (*A* and *B* on the N-terminal domain, *C* and *D* on the C-terminal domain, with no sequential order being implied within the domains). Each of the states and each of the reactions was explicitly modelled, with distinct dissociation constants for each of the sites. The dissociation constants for the *R* state were $K^R_{d_A} = 8.32 \times 10^{-6}$ M, $K^R_{d_B} = 1.66 \times 10^{-8}$ M, $K^R_{d_C} = 1.74 \times 10^{-5}$ M, and $K^R_{d_D} = 1.45 \times 10^{-8}$M. According to this model, $L = 20670$, and $c = 0.00396$ for all four binding sites [8]. The calmodulin concentration used for the model was 2×10^7 M [8], and simulations were run using COPASI [9].

When the fractional occupancy of calmodulin is plotted against initial free calcium concentration, simulation outcomes seem to agree quite well with experimental observations [8], but such a plot does not provide a direct way of quantifying this agreement.

To do this, we inserted the parameters of the MWC model into equations 8 to 11 to obtain Adair-Klotz constants. These can be compared to Adair-Klotz constants previously obtained in experimental studies [10-14], as listed in Table 1. This comparison shows that all four Adair-Klotz constants computed from the general MWC model lie within the experimentally reported range, and thus show that the MWC model is indeed consistent with experimental data.

Table 1: Apparent Adair-Klotz constants for the calmodulin model

	this paper	reported range
K_1	5.1860×10^5	1.16×10^5 [11] – 1.7×10^6 [11]
K_2	5.1601×10^5	1.4×10^5 [11] – 8.9×10^5 [12]
K_3	1.3377×10^5	2.86×10^4 [13] – 2.9×10^6 [11]
K_4	3.8784×10^4	1.7×10^3 [14] – 1.12×10^5 [13]

Apparent Adair-Klotz constants (in M) for the calmodulin model as computed with our method, and comparison to several experimental reports [10-14] and data reviews [11].

Figure 1 visualises this comparison: The Adair-Klotz curve obtained from the MWC model is compared to experimental measurements done by Porumb [12], Crouch and Klee [10], and Peersen *et al*. [15] and to an Adair-Klotz fit to the combination of all three data sets. The plot illustrates that the Adair curve obtained from the parameters of the generalised MWC model presented here is similar to that obtained from experimental data, and that computing an Adair-Klotz function from the parameters of a MWC model does indeed provide a way of comparing an allosteric model to experimental measurements.

Allosteric model of Hemoglobin

In a similar manner, the case in which all binding sites are equivalent [7] can be seen as a special case, in which there is only one sub-group of identical binding sites. With four binding sites, as is the case for hemoglobin, we obtain:

$$K_1 = 4\frac{K^R + LK^T}{1 + L} \tag{18}$$

$$K_2 = \frac{3}{2}\frac{(K^R)^2 + L(K^T)^2}{K^R + LK^T} \tag{19}$$

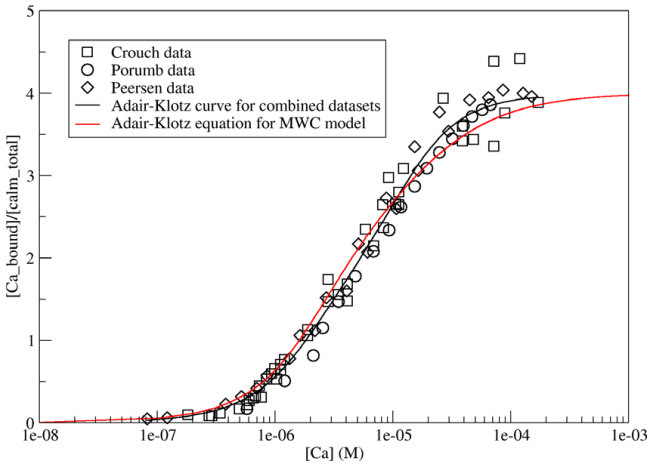

Figure 1
Comparison of the calmodulin model with experimental data. Red curve shows the Adair-Klotz equation using the Adair-Klotz constants obtained from the MWC model of calmodulin. Symbols are used to represent data points from various experimental measurements of calmodulin binding to calcium: Circles for Porumb [12], squares for Crouch and Klee [10], diamonds for Peersen *et al.* [15]. The black line represents a fit of all of these data set to the Adair-Klotz equation, which was obtained using the "Non-linear curve-fitting" function in grace http://plasma-gate.weizmann.ac.il/Grace/.

$$K_3 = \frac{2}{3}\frac{(K^R)^3 + L(K^T)^3}{(K^R)^2 + L(K^T)^2} \quad (20)$$

$$K_4 = \frac{1}{4}\frac{(K^R)^4 + L(K^T)^4}{(K^R)^3 + L(K^T)^3} \quad (21)$$

Yonetani *et al*. [16] fitted the same data for hemoglobin binding to oxygen once using the MWC framework and once using the Adair-Klotz framework. This study provides an excellent opportunity to test the validity of the conversion equations presented here: By using the results of their MWC fit and inserting K_R, K_T, and L into the equations presented in [7], we get an independent determination of the Adair-Klotz constants K_1 to K_4. Table 2 compares the Adair-Klotz constants thus obtained to the Adair-Klotz constants obtained by Yonetani *et al*. [16]. Both methods yield essentially the same results, slight differences are presumably due to rounding errors and/or to limitations of the data fitting algorithms used, as well as possible over-fitting in the case of the Adair-Klotz framework.

Discussion and conclusion

The generalised MWC model proposed here opens up new ways of applying the allosteric framework: Not only to multimers consisting of identical subunits with one ligand binding site on each, but also to proteins with several binding sites of different affinities for the same ligand, be it multimers with more than one binding site on each subunit or monomeric proteins containing several binding sites. This framework has been used for an allosteric model of calmodulin [8], and could be useful in the analysis of a wide range of other proteins.

Table 2: Comparison of MWC and Adair-Klotz constants for hemoglobin

	this paper	Yonetani *et al*. [16]
K_1	7.68×10^{-3}	7.20×10^{-3}
K_2	0.96×10^{-2}	1.05×10^{-2}
K_3	1.52×10^{-2}	1.15×10^{-2}
K_4	2.32×10^{-2}	2.33×10^{-2}

Experimental and theoretical determination of Adair-Klotz constants (in $torr^{-1}$) from MWC constants at pH 7.0. $K_R = 3.0 \times 10^{-2} torr^{-1}$, $K_T = 7.0 \times 10^{-3}$ $torr^{-1}$, and $L = 33$, as obtained by Yonetani *et al*. by fitting data with an MWC equation [16]. We used these to compute K_1 to K_4 using the equations presented in [7] and here compare them to K_1 to K_4 obtained by Yonetani *et al*. by fitting the same data with an Adair-Klotz equation [16]. Note that Yonetani *et al*. used a slightly modified version of the Adair-Klotz equation, meaning that K_1 in [16] corresponds to $\frac{1}{4}K_1$ in [4], K_2 in [16] to $\frac{2}{3}K_2$ in [4], K_3 in [16] to $\frac{3}{2}K_3$ in [4] and K_4 in [16] to $4K_4$ in [4]. To allow easier comparability, we used Yonetani's notation for this table and labelled the constants $K_1', \ldots, K_2'$ to avoid confusion with the original Klotz notation used everywhere else in this paper.

Other generalisations of the MWC framework have been presented in the past. Mello and Tu [17] have proposed a heterogeneous MWC (HMWC) model for allosteric proteins or protein complexes that bind to different types of ligand (but where there is only one affinity per ligand). This can easily be combined with the model presented here: The fractional occupancy for a generalised heterogeneous protein with two different types of ligand, and binding sites of different affinity for each ligand, would be:

$$\bar{Y} = \frac{1}{n}\left(\frac{\left(\sum_{i=1}^{n_1}\left([X_1]K_i^R\prod_{j\neq i}(1+[X_1]K_j^R)\right)\right)\left(\sum_{i=1}^{n_2}\left([X_2]K_i^R\prod_{j\neq i}(1+[X_2]K_j^R)\right)\right)}{\prod_{i=1}^{n_1}(1+[X_1]K_i^R)\prod_{i=1}^{n_2}(1+[X_2]K_i^R)+L\prod_{i=1}^{n_1}(1+c_i[X_1]K_i^R)\prod_{i=1}^{n_2}(1+c_i[X_2]K_i^R)} + \frac{L\left(\sum_{i=1}^{n_1}(c_i[X_1]K_i^R\prod_{j\neq i}(1+c_j[X_1]K_j^R))\right)\left(\sum_{i=1}^{n_2}(c_i[X_2]K_i^R\prod_{j\neq i}(1+c_j[X_2]K_j^R))\right)}{\prod_{i=1}^{n_1}(1+[X_1]K_i^R)\prod_{i=1}^{n_2}(1+[X_2]K_i^R)+L\prod_{i=1}^{n_1}(1+c_i[X_1]K_i^R)\prod_{i=1}^{n_2}(1+c_i[X_2]K_i^R)} \right) \quad (22)$$

where $[X_1]$ represents the first ligand, for which n_1 binding sites exist, and $[X_2]$ the second ligand, for which there are n_2 binding sites. For a heterogeneous complex with m types of ligands, the equation is

$$\bar{Y} = \frac{1}{n}\frac{\prod_{k=1}^{m}\left(\sum_{i=1}^{n_k}\left([X_k]K_i^R\prod_{j\neq i}(1+[X_k]K_j^R)\right)\right)+L\prod_{k=1}^{m}\left(\sum_{i=1}^{n_k}\left(c_i[X_k]K_i^R\prod_{j\neq i}(1+c_j[X_k]K_j^R)\right)\right)}{\prod_{k=1}^{m}\prod_{i=1}^{n_k}(1+[X_k]K_i^R)+L\prod_{k=1}^{m}\prod_{i=1}^{n_k}(1+c_i[X_k]K_i^R)} \quad (23)$$

The case in which binding sites for a given ligand can be grouped into sets of same affinity is straight-forward, as is the computation of fractional occupancy, R.

Najdi *et al*. [18] have proposed a generalised MWC (GMWC) model for a protein binding to several ligand types and regulated by multiple allosteric activators or inhibitors. This model can be combined with the model presented here by replacing the term that denotes substrate concentration and affinity for each ligand in [18] by the appropriate sum: in the notation employed by [18], this would mean replacing $\left(1+\frac{[S_q]}{K_{Mq}}\right)^n$ by $\left(\prod_{i=1}^{n}\left(1+\frac{[S_q]}{K_{Mqi}}\right)\right)$ for each ligand. Such a combined model could then cater for proteins that bind to several ligand types (with non-identical binding sites per ligand)

and that are regulated by multiple allosteric activators or inhibitors.

In biology, the same question can be tackled at different levels and with different approaches, often based on different underlying theoretical framework. These approaches, however, need to be comparable to allow for cross-validation and for the assembly of different types of data into a comprehensive understanding of a given process. For instance, computational modellers need a way of comparing their models with experimental results to assess the validity of their models. In particular, mechanistic models need to be comparable to data or to the phenomenological models describing them. We offer a way of relating intrinsic association constants in allosteric models to Adair-Klotz constants and thus to bridge the gap between generalised allosteric models and experimental observations.

Apart from enabling modellers to validate their models – as shown here in the two example cases – these conversion equations could also help in model construction by providing ways to constrain parameter space and facilitate the estimation of allosteric parameters, which is very useful in cases where there is little or no additional experimental evidence that could help with their derivation.

Abbreviations

MWC: Monod-Wyman-Changeux; R: relaxed; T: tense.

Authors' contributions

MIS designed the generalised MWC framework and wrote the conversion equations with the help of SJE. All authors contributed to the manuscript. All authors read and approved the final manuscript.

References

1. Wyman J, Gill SJ: *Binding and linkage. Functional chemistry of biological molecules* University Science Books, Mill Valley; 1990.
2. Hill AV: **The possible effects of the aggregation of the molecules of hæmoglobin on its dissociation curves.** *J Physiol* 1910, **40:**iv-vii.
3. Adair GS: **The hemoglobin system. IV. The oxygen dissociation curve of hemoglobin.** *J Biol Chem* 1925, **63:**529-545.
4. Klotz IM: **The Application of the Law of Mass Action to Binding by Proteins. Interactions with Calcium.** *Arch Biochem* 1946, **9:**109-117.
5. Klotz IM: **Ligand-receptor complexes: origin and development of the concept.** *J Biol Chem* 2004, **279:**1-12.
6. Monod J, Wyman J, Changeux JP: **On the Nature of Allosteric Transitions: A Plausible Model.** *J Mol Biol* 1965, **12:**88-118.
7. Edelstein SJ: **Cooperative interactions of hemoglobin.** *Annu Rev Biochem* 1975, **44:**209-232.
8. Stefan MI, Edelstein SJ, Le Novère N: **An allosteric model of calmodulin explains differential activation of PP2B and CaMKII.** *Proc Natl Acad Sci USA* 2008, **105(31):**10768-10773.
9. Hoops S, Sahle S, Gauges R, Lee C, Pahle J, Simus N, Singhal M, Xu L, Mendes P, Kummer U: **COPASI-a COmplex PAthway SImulator.** *Bioinformatics* 2006, **22(24):**3067-3074.
10. Crouch TH, Klee CB: **Positive cooperative binding of calcium to bovine brain calmodulin.** *Biochemistry* 1980, **19(16):**3692-3698.
11. Burger D, Cox JA, Comte M, Stein EA: **Sequential Conformational Changes in Calmodulin upon Binding of Calcium.** *Biochemistry* 1984, **23:**1966-1971.
12. Porumb T: **Determination of calcium-binding constants by ow dialysis.** *Anal Biochem* 1994, **220(2):**227-237.
13. Shifman JM, Choi MH, Mihalas S, Mayo SL, Kennedy MB: **Ca2+/calmodulin-dependent protein kinase II (CaMKII) is activated by calmodulin with two bound calciums.** *Proc Natl Acad Sci USA* 2006, **103(38):**13968-13973.
14. Haiech J, Klee CB, Demaille JG: **Effects of cations on affinity of calmodulin for calcium: ordered binding of calcium ions allows the specific activation of calmodulin-stimulated enzymes.** *Biochemistry* 1981, **20(13):**3890-3897.
15. Peersen OB, Madsen TS, Falke JJ: **Intermolecular tuning of calmodulin by target peptides and proteins: differential effects on Ca2+ binding and implications for kinase activation.** *Protein Sci* 1997, **6(4):**794-807.
16. Yonetani T, Park SI, Tsuneshige A, Imai K, Kanaori K: **Global allostery model of hemoglobin. Modulation of O(2) affinity, cooperativity, and Bohr effect by heterotropic allosteric effectors.** *J Biol Chem.* 2002, **77(37):**34508-34520.
17. Mello BA, Tu Y: **An allosteric model for heterogeneous receptor complexes: understanding bacterial chemotaxis responses to multiple stimuli.** *Proc Natl Acad Sci USA* 2005, **102(48):**17354-17359.
18. Najdi TS, Yang CR, Shapiro BE, Hatfield GW, Mjolsness ED: **Application of a generalized MWC model for the mathematical simulation of metabolic pathways regulated by allosteric enzymes.** *J Bioinform Comput Biol* 2006, **4(2):**335-355.

OPEN ACCESS Freely available online

PLoS one

Structural Analysis and Stochastic Modelling Suggest a Mechanism for Calmodulin Trapping by CaMKII

Melanie I. Stefan[¤a], David P. Marshall[¤b], Nicolas Le Novère*

EMBL-European Bioinformatics Institute, Hinxton, UK

Abstract

Activation of CaMKII by calmodulin and the subsequent maintenance of constitutive activity through autophosphorylation at threonine residue 286 (Thr286) are thought to play a major role in synaptic plasticity. One of the effects of autophosphorylation at Thr286 is to increase the apparent affinity of CaMKII for calmodulin, a phenomenon known as ''calmodulin trapping''. It has previously been suggested that two binding sites for calmodulin exist on CaMKII, with high and low affinities, respectively. We built structural models of calmodulin bound to both of these sites. Molecular dynamics simulation showed that while binding of calmodulin to the supposed low-affinity binding site on CaMKII is compatible with closing (and hence, inactivation) of the kinase, and could even favour it, binding to the high-affinity site is not. Stochastic simulations of a biochemical model showed that the existence of two such binding sites, one of them accessible only in the active, open conformation, would be sufficient to explain calmodulin trapping by CaMKII. We can explain the effect of CaMKII autophosphorylation at Thr286 on calmodulin trapping: It stabilises the active state and therefore makes the high-affinity binding site accessible. Crucially, a model with only one binding site where calmodulin binding and CaMKII inactivation are strictly mutually exclusive cannot reproduce calmodulin trapping. One of the predictions of our study is that calmodulin binding in itself is not sufficient for CaMKII activation, although high-affinity binding of calmodulin is.

Citation: Stefan MI, Marshall DP, Le Novère N (2012) Structural Analysis and Stochastic Modelling Suggest a Mechanism for Calmodulin Trapping by CaMKII. PLoS ONE 7(1): e29406. doi:10.1371/journal.pone.0029406

Editor: Christina Chan, Michigan State University, United States of America

Received July 26, 2011; **Accepted** November 28, 2011; **Published** January 18, 2012

Funding: These authors have no support or funding to report.

Competing Interests: The authors have declared that no competing interests exist.

¤a Current address: Biology Division, California Institute of Technology, Pasadena, California, United States of America
¤b Current address: Department of Biochemistry, University of Oxford, UK

* E-mail: lenov@ebi.ac.uk

Introduction

Calcium/calmodulin-dependent kinase II (CaMKII) [1], a highly abundant neuronal protein, has been implicated in learning and memory. Knockout mice that cannot express the α isoform of CaMKII show deficiencies in spatial learning [2] and also in hippocampal long-term potentiation (LTP) [3]. Long-term potentiation is an activity-dependent increase in synaptic strength [4] that has long been associated with learning and memory [4,5]. On a molecular level, the coincident activity of a pair of neurons triggers a calcium signalling cascade that will lead to a strengthening of the synaptic connection: Upon activation of AMPA receptors by glutamate, the postsynaptic neuron is depolarised, relieving the Mg^{2+} block that inhibits NMDA receptor function under basal conditions [6,7]. The resulting calcium influx through the NMDA receptor leads to the activation of CaMKII via calmodulin [8–10]. Active CaMKII enhances the function of AMPA receptor channels by phosphorylating their GluR1 subunit [11]. It also mediates an increase of AMPA receptor delivery to the postsynaptic membrane [12]. The role of CaMKII in postsynaptic calcium signalling and its abundance in neurons support the view that CaMKII is a key protein in LTP induction and learning.

The CaMKII holoenzyme is dodecameric, organised as a hexamer of dimers [13] with the appearance of two stacked rings [14]. Each subunit can adopt two distinct conformations: An autoinhibited ''closed'' conformation, in which the active site is bound to the auto-inhibitory helix [13], and an active ''open'' conformation, in which this interaction is disrupted. Calmodulin stabilises CaMKII activity by binding to the inhibitory helix [15]. The open state of CaMKII is further stabilised by autophosphorylation at threonine residue 286 (Thr286) [16], which confers calmodulin-independent activity [17]. Phosphorylation at Thr286 increases the apparent affinity of CaMKII for calmodulin [18]. This is due to a decrease in the rate at which calmodulin dissociates. A mechanistic explanation for this phenomenon, called ''calmodulin trapping'', is yet to be found. It has been suggested, however, that the phenomenon of calmodulin trapping might be related to the existence of two calmodulin binding sites on each CaMKII subunit: one high-affinity binding site within residues 291–312 and one low-affinity binding site within residues 298–312 [19].

In order to better understand the molecular basis of calmodulin trapping, we used a combination of structural modelling and stochastic simulations of CaMKII regulation. We show here that calmodulin binding in itself is not sufficient for CaMKII activation, and that calmodulin trapping can be explained by the existence of two binding sites.

Several models of various aspects of CaMKII function exist. Some of these have not included calmodulin trapping at all, because they were concerned with other aspects of CaMKII function, such as frequency dependence [20] or bistability [21–

23]. Models that did include calmodulin trapping (e.g. [24–27]) have modelled it explicitly, as an ad hoc change in calmodulin affinity once a CaMKII subunit is phosphorylated. Our model is the first one to offer a mechanistic explanation of calmodulin trapping.

Results

To investigate whether binding of calmodulin to the presumed high-affinity binding site was structurally plausible and to investigate the effect that this would have on the CaMKII subunit, we turned to structural modelling.

Closed and open conformations explored in the absence of Calmodulin

We first investigated the range of conformations a single CaMKII subunit can explore if it is allowed to open up, i.e. if the linking region between the inhibitory helix and the rest of the kinase domain is allowed some flexibility. We used a previously published structure of the CaMKII kinase domain from *C. elegans* CaMKII (PDB ID: 2BDW, chain A) [13] and performed structural modelling where information about the four residues that link the inhibitory helix to the active domain were left out. An overlay of 100 structures is shown in Figure 1, and average root-mean-square deviation (RMSD) for each residue is plotted in Figure 2. In the absence of further constraints, the flexible linker allows for considerable movement of the inhibitory helix with respect to the kinase domain, ranging from structures which are essentially closed, i. e. where the catalytic domain is masked by the auto-inhibitory helix, to open structures, where the kinase domain is accessible. This is consistent with a recent study by Hoffman et al. who found that in the absence of calmodulin, CaMKII exists as a conformeric equilibrium between structures where the auto-inhibitory helix and the kinase domain interact and structures where this interaction is disrupted [28].

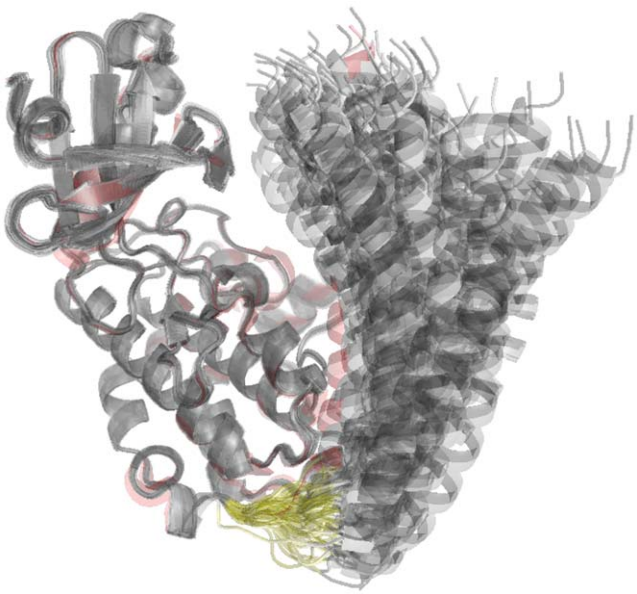

Figure 1. Opening of a CaMKII subunit. Overlay of 100 model structures created with MODELLER, where structural information was omitted for the four residues linking the kinase domain of CaMKII with the inhibitory helix. These four residues are shown in yellow. The structure corresponding to the published structure of the kinase domain (with the linker region intact, PDB ID: 2BDW, chain A) [13] is shown in red.
doi:10.1371/journal.pone.0029406.g001

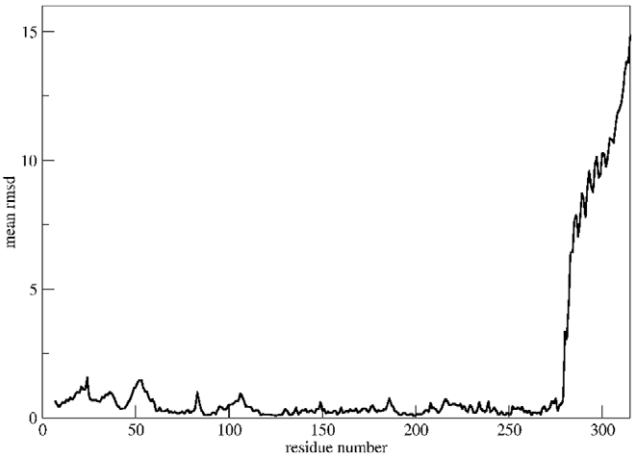

Figure 2. Opening of a CaMKII subunit: Mean RMSD per residue. Average root-mean-square deviation (RMSD) per residue for the structures shown in figure 1. RMSD values were computed using Chimera [53].
doi:10.1371/journal.pone.0029406.g002

Low-affinity binding of calmodulin does not interfere with the closed conformation of CaMKII

To model the structure of calmodulin bound to the low-affinity binding site of CaMKII, we used previously published structures of the kinase domain of CaMKII (PDB ID: 2BDW, chain A) [13] and of calmodulin bound to a fragment of the inhibitory helix of CaMKII (PDB ID: 1CM1, chains A and B) [29] for structural modelling and molecular dynamics simulations. The structural model suggests that calmodulin binding to the low-affinity binding site of CaMKII is compatible with closure of the CaMKII subunit (see Figure 3, left panel). A PDB file of the resulting structure can be found in Dataset S1.

To test whether low-affinity binding of calmodulin to CaMKII might favour a more open structure, we gave the inhibitory helix of CaMKII freedom to move by introducing a flexible linker between the helix and the kinase domain. The model suggests that even if the inhibitory helix is given freedom to move away from the catalytic domain, the closed form is preferred (see Figure 3, right panel). This may be due to an interaction between residues Asp51 and Asp59 in the calmodulin structure (PDB ID: 1CM1, chain A) and Lys20 (in *C. elegans*, corresponding to Lys21 in mouse or rat) in the catalytic domain of CaMKII (PDB ID: 2BDW, chain A). The interaction is highlighted in Figure 4. A similar interaction between calmodulin and the catalytic kinase domain has recently been reported for calmodulin binding to death-associated protein kinase (DAPK) [30]. In the absence of this interaction, low-affinity binding of calmodulin would be compatible with further opening of the CaMKII subunit. This would be the case, for instance, when CaMKII is locked in the open conformation by autophosphorylation at Thr286. A structure of calmodulin bound to an open conformation of CaMKIIδ has indeed been observed (PDB ID: 2WEL) [31].

Thus, the structural model suggests that calmodulin binding to the low-affinity binding site on CaMKII can happen independently of whether the CaMKII subunit is open or closed. This would also mean that binding of calmodulin does not necessarily stabilise the active conformation of CaMKII, at least as long as calmodulin is bound to the low-affinity site.

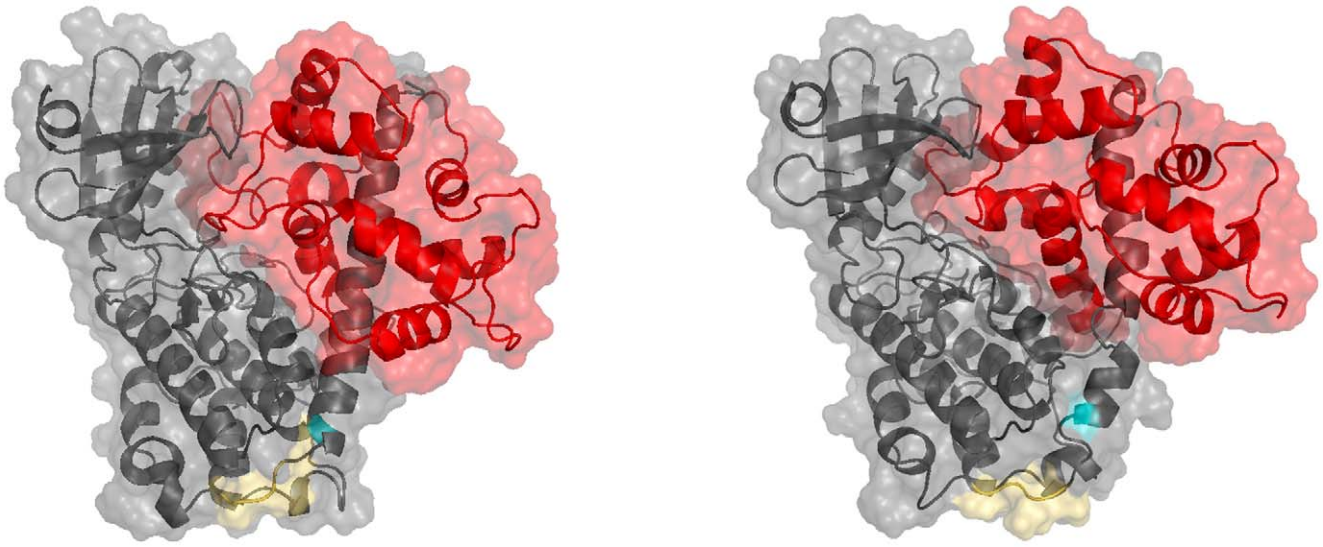

Figure 3. Models of Calmodulin bound to the low-affinity site of a CaMKII subunit. Left panel: Binding to a CaMKII subunit in a closed conformation. Right panel: Binding to a CaMKII subunit with flexible linker. Although the linker region between inhibitory helix and catalytic domain was flexible, the complex CaMKII-calmodulin still favoured a closed conformation of CaMKII. Calmodulin is shown in red, CaMKII in grey. The Thr286 autophosphorylation site is shown in teal, the region that links the catalytic domain to the autoinhibitory helix in yellow.
doi:10.1371/journal.pone.0029406.g003

High-affinity binding of calmodulin requires opening of CaMKII

In order to model calmodulin binding to the high-affinity binding site on CaMKII, we modified the structure of calmodulin bound to a fragment of the inhibitory helix of CaMKII (PDB ID: 1CM1, chains A and B) [29] by manually shifting the position of calmodulin by one turn of the helix, corresponding to the supposed position of the high-affinity binding site. We then used this structure and the structure of the kinase domain of CaMKII (PDB ID: 2BDW, chain A) [13] to create a combined structural model. This approach, however, failed to give a valid structure without overlaps. We concluded that calmodulin binding to the proposed high-affinity binding site is impossible if CaMKII is in the closed conformation.

To further test this hypothesis, we repeated our modelling approach, this time omitting structural information pertaining to the linker region between the inhibitory helix and the kinase domain, so that the two domains were free to move with respect to each other. Under these conditions we could indeed obtain an overlap-free structure of the calmodulin-CaMKII complex (see Figure 5). A PDB file of this structure is provided in Dataset S2.

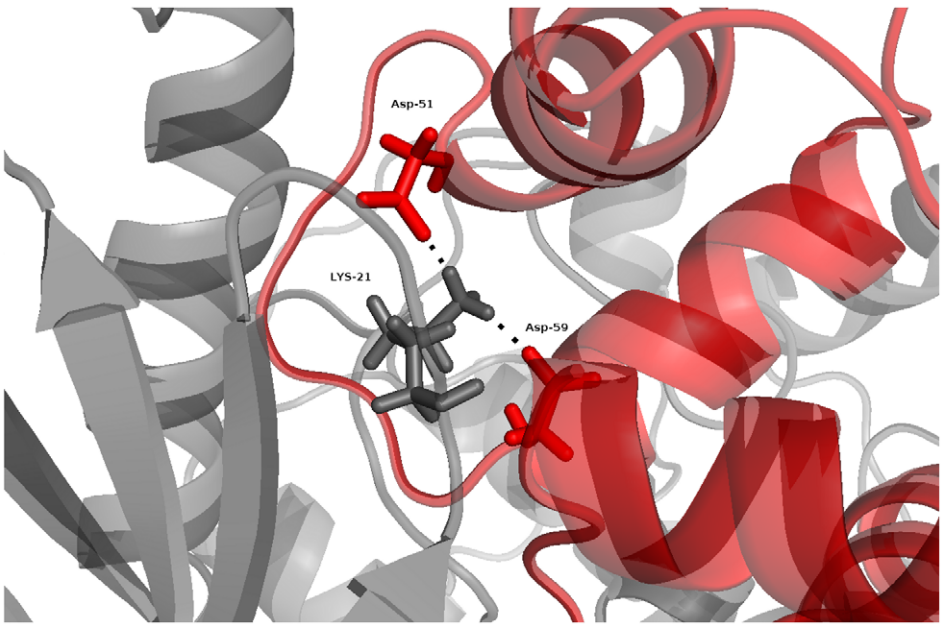

Figure 4. Interactions between calmodulin and its low-affinity binding site on the kinase domain of CaMKII. Interacting residues are shown as sticks. Calmodulin is shown in red and CaMKII in grey.
doi:10.1371/journal.pone.0029406.g004

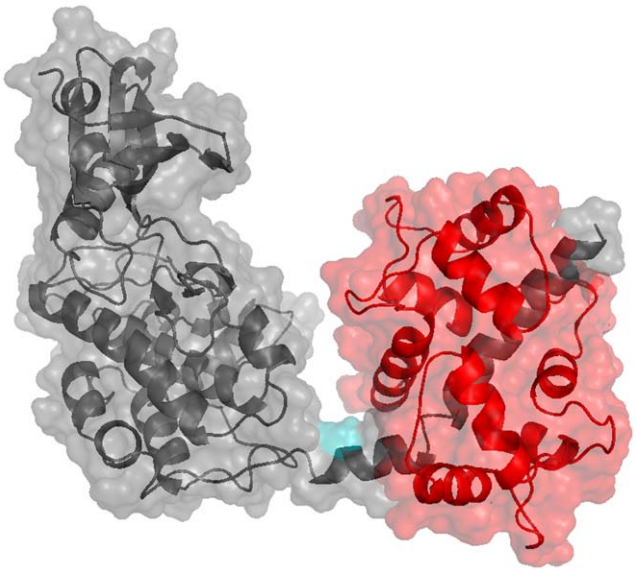

Figure 5. High-affinity binding of calmodulin to the open state of CaMKII. Calmodulin is shown in red, CaMKII in grey and the autophosphorylation site at Thr286 in teal.
doi:10.1371/journal.pone.0029406.g005

It is interesting to note that this structure requires a considerable degree of opening of the CaMKII subunit, thereby exposing the autophosphorylation site at Thr286. Unlike in the model of calmodulin binding to the low-affinity site, there seems to be no interaction between calmodulin and the catalytic domain of CaMKII, which allows CaMKII to adopt an open state and facilitates substrate access to the catalytic site. In addition, calmodulin binding to the high-affinity site seems to cause some degree of local conformational change in the inhibitory helix.

Together, these results suggest that binding of calmodulin to the low-affinity site is independent on whether CaMKII is open or closed, but that binding to the high-affinity site requires opening of CaMKII, and will therefore stabilise the active open state.

High-affinity binding includes residues crucial for calmodulin trapping

Having obtained a structural model of calmodulin binding to an open state of CaMKII, we examined whether this structure could be relevant for calmodulin trapping. By using site-directed mutagenesis, Singla et al. [32] have shown residues Phe293 on CaMKII and Glu120 and Met124 on calmodulin to be crucial for calmodulin trapping by CaMKII. Indeed, in the high-affinity structure, Met124 on calmodulin makes contact with both Phe293 on CaMKII and Glu120 on calmodulin (see Figure 6, left panel), a feature not found in the low-affinity structure (see Figure 6, right panel).

This suggests that binding of calmodulin to the high-affinity site on CaMKII may play an important role in calmodulin trapping.

Only one calmodulin binding site can be occupied at any given time

The structural model also suggests that, although there might well be two binding sites for calmodulin on each CaMKII subunit, no more than one calmodulin molecule can be bound at any given time. Figure 7 shows that there is considerable overlap between the two binding sites. This means that the actual stoichiometry of CaMKII binding to calmodulin is still at most one calmodulin bound per subunit of CaMKII. Due to the proximity of the two binding sites, however, calmodulin binding to the low-affinity site will greatly increase the effective local concentration of calmodulin around the high-affinity binding site, and vice versa. Thus, a calmodulin molecule could effectively stay associated with a CaMKII subunit, while "sliding" back and forth between the low-affinity and the high-affinity binding site.

Thus, the two binding sites for calmodulin on CaMKII do not allow more than one calmodulin molecule to bind at any given time, but provide two modes of binding to CaMKII for a single calmodulin molecule.

The structural model is compatible with a two-binding-sites hypothesis

Taken together, the results suggest that the structural model of calmodulin binding to CaMKII is indeed compatible with the existence of two calmodulin binding sites on CaMKII, as suggested by Tse et al. [19]. Binding to one of these sites (the low-affinity site) would be compatible with closure and hence, inactivity of the CaMKII subunit, while binding to the other (high-affinity) site would require CaMKII to be open. The presumed high-affinity binding event involves residues previously implied in calmodulin trapping [32]. To test whether this two-binding-sites model could explain calmodulin trapping by autophosphorylated CaMKII, we set up a stochastic model of these interactions.

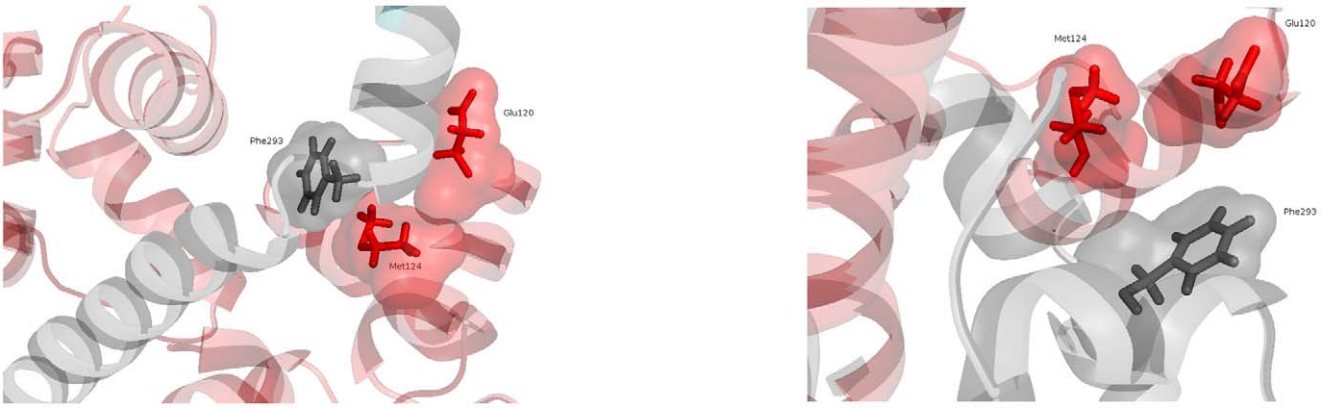

Figure 6. Residues crucial for calmodulin trapping. Left panel: In the high-affinity structure, residue Met124 on calmodulin (in red) makes contact both with residue Glu120, also on calmodulin and with residue Phe293 on CaMKII (in grey). Right panel: In the low-affinity structure, these contacts are missing.
doi:10.1371/journal.pone.0029406.g006

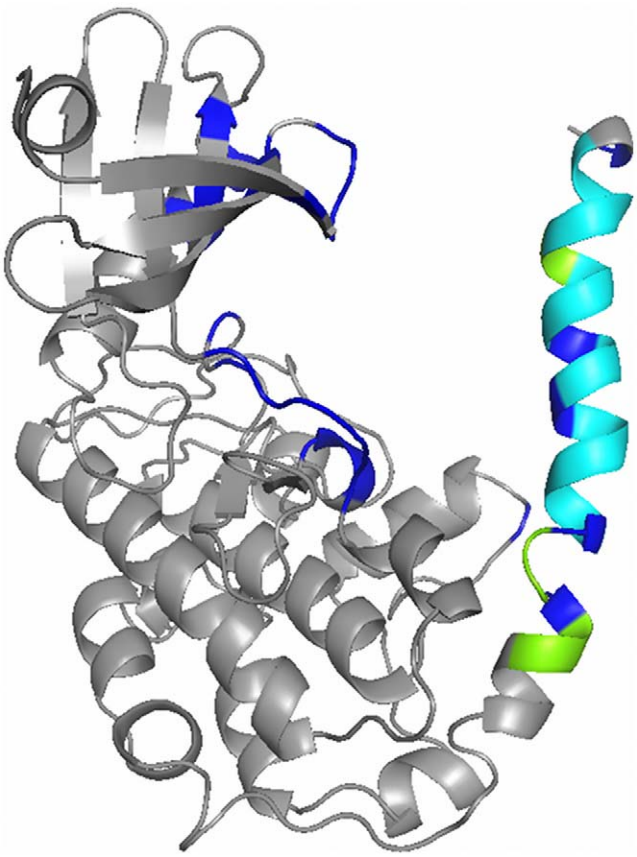

Figure 7. Interaction surfaces for low-affinity and high-affinity binding. The interaction surfaces for calmodulin binding are projected onto a CaMKII monomer. The low-affinity interaction surface is shown in blue, the high-affinity interaction surface in green, and the overlap in cyan. Interaction surfaces were computed using Chimera [53] with a 6Å cutoff.
doi:10.1371/journal.pone.0029406.g007

Stochastic simulations of calmodulin trapping by CaMKII

Using the results from structural modelling, we have designed a rule-based model of calmodulin trapping by CaMKII. In this model, CaMKII is represented as a hexamer. This is a compromise between modelling CaMKII as a collection of monomeric subunits and modelling CaMKII as a dodecameric holoenzyme. A model in which CaMKII is represented as unconnected monomeric subunits would be sufficient in order to study the core mechanisms for calmodulin trapping (including the two binding sites for calmodulin, opening and closing of the subunit and the effect of Thr286 phosphorylation on calmodulin affinity). However, it would make it harder to accurately describe Thr286 autophosphorylation, which is a neighbour-sensitive reaction between adjacent subunits on the same hexameric ring. On the other hand, representing CaMKII as a full dodecamer would make it necessary to include other kinds of neighbour-sensitive interactions - many of them as yet poorly understood - but would not provide any additional insights into the trapping mechanism.

In our model, each subunit of CaMKII can be open or closed, phosphorylated at threonine residues 286 and 306 and bound to calmodulin on either the high-affinity or the low-affinity binding site. The open form is assumed to be catalytically active. This results in a model where each subunit has five binary state flags: activity, phosphorylation at Thr286, phosphorylation at Thr306, binding of calmodulin to either of the two sites and binding of calmodulin to the high-affinity site. (The last two flags are set to 00 if no calmodulin is bound, 10 if calmodulin is bound to the low-affinity site and 11 if calmodulin is bound to the high-affinity site. The combination 01 is impossible.) Autophosphorylation at Thr286 is modelled as a neighbour-sensitive reaction, which can only occur if both the subunit acting as the kinase and the subunit acting as the substrate for the phosphorylation reaction are open. Phosphorylation at Thr286 locks a subunit in the open state. In our model, the corresponding dephosphorylation is mediated protein phosphatase 1 (PP1). Phosphorylation at Thr306 is an intra-subunit autophosphorylation and therefore depends on the subunit in question being active. Phosphorylation at this residue, however, does not interfere with closing of the subunit. Since both the presumed high-affinity and low-affinity binding domains for calmodulin contain residue Thr306, phosphorylation at this residue and calmodulin binding are modelled to be mutually exclusive. Following the results of the structural model presented above, calmodulin binding to the high-affinity binding site precludes closing of a CaMKII subunit, whereas binding to the low-affinity site does not interfere with closing.

A diagram of the reaction scheme used in the stochastic model can be found in Figure 8. A full list of reaction rules is given in table 1.

The two-binding-sites model can reproduce trapping

To assess whether our model can reproduce the trapping of calmodulin observed in vitro, we ran stochastic simulations on both wildtype CaMKII and an in silico mutant version that cannot be phosphorylated at Thr286. Following the experimental procedure of Meyer et al. [18], the system was allowed to saturate for thirty seconds, and calmodulin then inactivated, corresponding to the withdrawal of calcium in the experimental setup. The ratio between calmodulin and CaMKII concentration used for this simulation was the same as used by Meyer et al. [18] (60 hexamers of CaMKII for 450 molecules of calmodulin), and no phosphatase was present. To ensure that the observed result is not just a random effect, the same simulation was repeated ten times on wildtype and mutant CaMKII. The simulations (see Figure 9) show that although both versions of CaMKII were equally saturated with calmodulin after thirty seconds, calmodulin

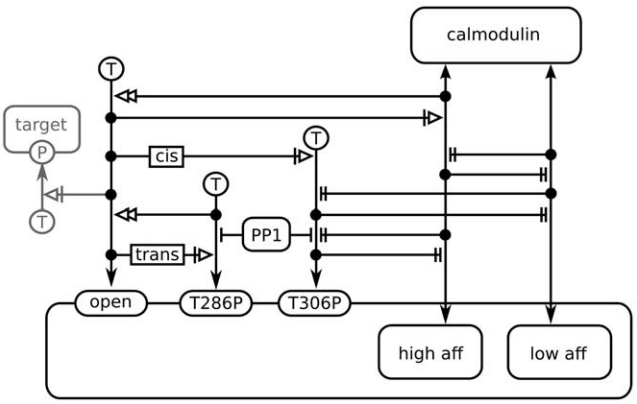

Figure 8. Model of calmodulin trapping by CaMKII. The model is shown as an SBGN ER diagram [54]. For clarity, only one monomeric subunit is shown. In the actual model, six such subunits form a ring, and autophosphorylation at Thr286 of one subunit is dependent on the neighbouring subunit being open.
doi:10.1371/journal.pone.0029406.g008

Table 1. List of reactions for the model of calmodulin trapping by CaMKII.

Phosphorylation of CaMKII at Thr286	Substrate: CaMKII Product: CaMKII Sets flag on neighbour: +P286 Needs flag: +open Needs flags on neighbour: +open −P286
Dephosphorylation of CaMKII at Thr286 by PP1	Substrates: CaMKII, PP1 Products: CaMKII, PP1 Sets flag: −P286 Needs flag: +P286
Phosphorylation of CaMKII at Thr306	Substrate: CaMKII Product: CaMKII Sets flag: +P306 Needs flags: +open −P306 –calm
Dephosphorylation of CaMKII at Thr306 by PP1	Substrates: CaMKII, PP1 Products: CaMKII, PP1 Sets flag: −P306 Needs flag: +P306
Calmodulin binding to CaMKII (low-affinity site)	Substrates:CaMKII, calmodulin Product: CaMKII Sets flag: +calm Needs flags: −P306 -calm –ha
Calmodulin dissociating from CaMKII (low-affinity site)	Substrate: CaMKII Products: CaMKII, calmodulin Sets flag: −calm Needs flags: +calm –ha
Calmodulin binding to CaMKII (high-affinity site)	Substrates: CaMKII, calmodulin Product: CaMKII Sets flags: +calm +ha Needs flags: +open −P306 −calm −ha
Calmodulin dissociating from CaMKII (high-affinity site)	Substrate: CaMKII Products: CaMKII, calmodulin Sets flags: −calm −ha Needs flags: +calm +ha
Opening of CaMKII (rapid equilibrium)	Substrate: CaMKII Product: CaMKII Sets flag: +open Probability: 1 if +P286 or +ha, 0.004 else
"Sliding" of calmodulin to the high-affinity site (rapid equilibrium)	Substrate: CaMKII Product: CaMKII Sets flag: +ha Probability: 0.99997 if +open and +calm

List of reactions for the model of calmodulin trapping by CaMKII.
doi:10.1371/journal.pone.0029406.t001

dissociation proceeded slower from the wildtype than from the mutant, showing a trapping effect that is, indeed, due to different apparent off rates.

Figure 10 shows examples of calmodulin binding behaviour at the level of the individual subunit. From one of the ten simulation runs above, we chose fifteen subunits at random out of all subunit that undergo calmodulin binding during the course of the simulation and plotted calmodulin binding and phosphorylation over time. The Figure shows that calmodulin binding behaviour varies widely across subunits. Note that since calmodulin was inactivated after $30\,s$, no new binding events are seen from then on, so whether calmodulin is bound to a subunit depends entirely on dissociation. While direct dissociation from the high-affinity site does occur, movement of calmodulin from the high-affinity site to the low-affinity site and back again is more frequent, especially in phosphorylated subunits.

Taken together, this shows that the two-binding-sites model presented here can reproduce calmodulin trapping without having to postulate changes in microscopic association or dissociation parameters upon phosphorylation of CaMKII. The existence of these two binding sites for calmodulin is thus sufficient to explain calmodulin trapping.

A one-binding-site model cannot reproduce trapping

Could calmodulin trapping be explained by an alternative model? Our model relies on two key assumptions: First, that each CaMKII subunit has two calmodulin binding sites and second, that binding to the low-affinity binding site does not necessarily entail CaMKII opening and thus, activation. This naturally raises the question of whether a model that does not rely on these two assumptions could also reproduce calmodulin trapping.

In order to address this issue, we constructed a model of CaMKII with only one (high-affinity) calmodulin binding site. In this model, calmodulin binding and closing of a CaMKII subunit are mutually exclusive, meaning that calmodulin binding is sufficient for CaMKII activation. All other reactions and parameters are the same as in the model presented above. Figure 11 (left panel) shows the pooled results of ten simulations on wildtype CaMKII and on Thr286-to-alanine (T286A) mutant CaMKII with this alternative model. As in the trapping simulation

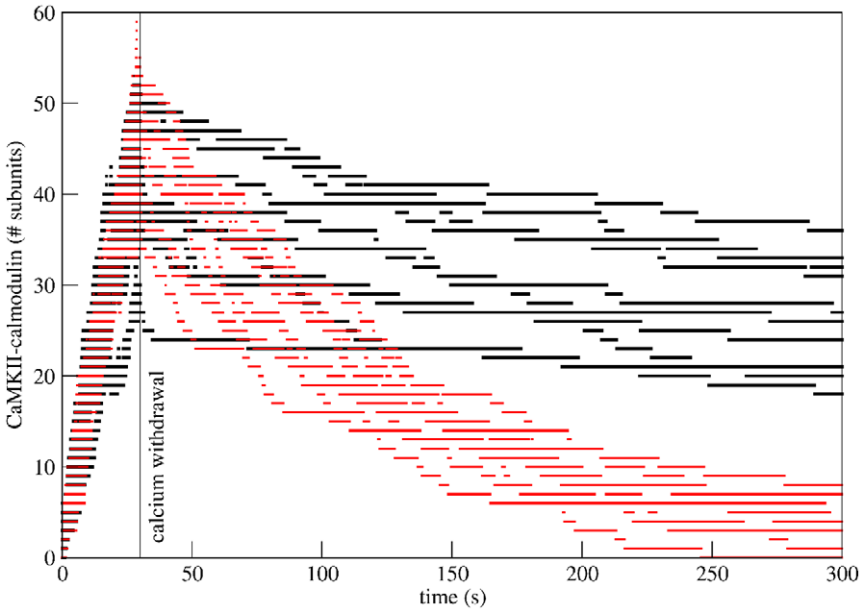

Figure 9. Several trapping simulations on wildtype and mutant CaMKII. Calmodulin is inactivated, mimicking calcium withdrawal after 30*s*. The ratio of calmodulin to CaMKII concentration used in the simulation was the same as used in the experimental setup by Meyer et al. [18]. The number of calmodulin-bound monomeric CaMKII subunits is plotted against time for each simulation run. The total number of CaMKII subunits in the simulation was 360. Wildtype is shown in black, T286A mutant in red. Ten simulation runs are shown for each.
doi:10.1371/journal.pone.0029406.g009

presented above, CaMKII was first saturated with calmodulin (here: at the beginning of the simulation in order to separate the effect of Thr286 on calmodulin binding from its effect on calmodulin dissociation) and all free calmodulin then withdrawn, such that dissociation of calmodulin from CaMKII could be monitored. The results show that this alternative model cannot reproduce the change in apparent k_{off} that characterises calmodulin trapping. For comparison, the same simulation was run with our two-binding-site model (Figure 11, right panel), showing a clear difference between wildtype and mutant CaMKII.

Taken together, these results suggest that the existence of two binding sites for calmodulin on a single CaMKII subunit is not only sufficient, but might indeed be necessary for trapping. If only one binding site is used in vivo, then another, yet unknown mechanism must be in place to enable calmodulin trapping.

Discussion

Assumptions underlying our model

The model presented above makes assumptions regarding both the choice of initial conditions for simulations and the fundamental mechanisms involved in calmodulin binding to CaMKII. Initial conditions were chosen to match the conditions used in the experimental paper that first reported calmodulin trapping [18]. This is why calmodulin concentration is saturating, the entire population of calmodulin molecules is assumed to be active at the beginning of the simulation and CaMKIIα is the only isoform considered. This reflects the situation in the test tube, and therefore, like an in vitro experiment, allows us to isolate and explain the particular mechanism of calmodulin trapping. This is also why the unit of analysis in our model is the hexameric ring, because, given our current knowledge, this is best suited to study calmodulin trapping: It includes the neighbour-sensitivity of Thr286 autophosphorylation, but disregards possibly confounding and as yet ill-understood effects of dodecameric assembly. In order to understand the role that calmodulin trapping plays in postsynaptic signalling and, ultimately, synaptic plasticity, it will be necessary to place the model in a context that better mimics in vivo conditions. This includes a more detailed representation of calmodulin activation, CaMKII topology and subunit composition, accurate calcium dynamics, the presence of other proteins and spine geometry.

Regarding the binding mechanisms, our model makes two important assumptions: First, that there are two binding sites for calmodulin on CaMKII and second, that binding to one of these sites is compatible with closing of CaMKII, i. e. that calmodulin binding is not sufficient for CaMKII activation. By measuring calmodulin binding to CaMKII peptides of different lengths, Waxham et al. [33] and Tse et al. [19] have made a plausible case for the first assumption, though whether both binding sites are actually used for calmodulin binding to full-length CaMKII in vivo has not been experimentally confirmed so far. (Note, however, that experimental work by Chin and Means [34] on full-length CaMKII seems to be consistent with the existence of two calmodulin binding sites, although the authors themselves do not draw the same conclusion). The second assumption is somewhat more controversial; in fact, most of the literature on CaMKII implicitly or explicitly assumes that calmodulin binding is sufficient for CaMKII activation (reviewed in [35]). The question therefore arises whether both these assumptions are necessary in order to reproduce trapping of calmodulin by CaMKII.

We therefore developed a corresponding one-binding-site model, where calmodulin binding is incompatible with CaMKII closing and therefore sufficient for CaMKII activation. This model has only one (high-affinity) binding site, and the apparent CaMKII affinity for calmodulin is slightly higher than for the wildtype in the two-binding-site model. This is because there is no exchange and no competition between high-affinity and low-affinity binding sites in the one-binding-site model, such that all calmodulin binding is concentrated on the high-affinity binding site. Crucially, this model could not reproduce calmodulin trapping: The apparent k_{off} of calmodulin is the same for wildtype and T286A mutant

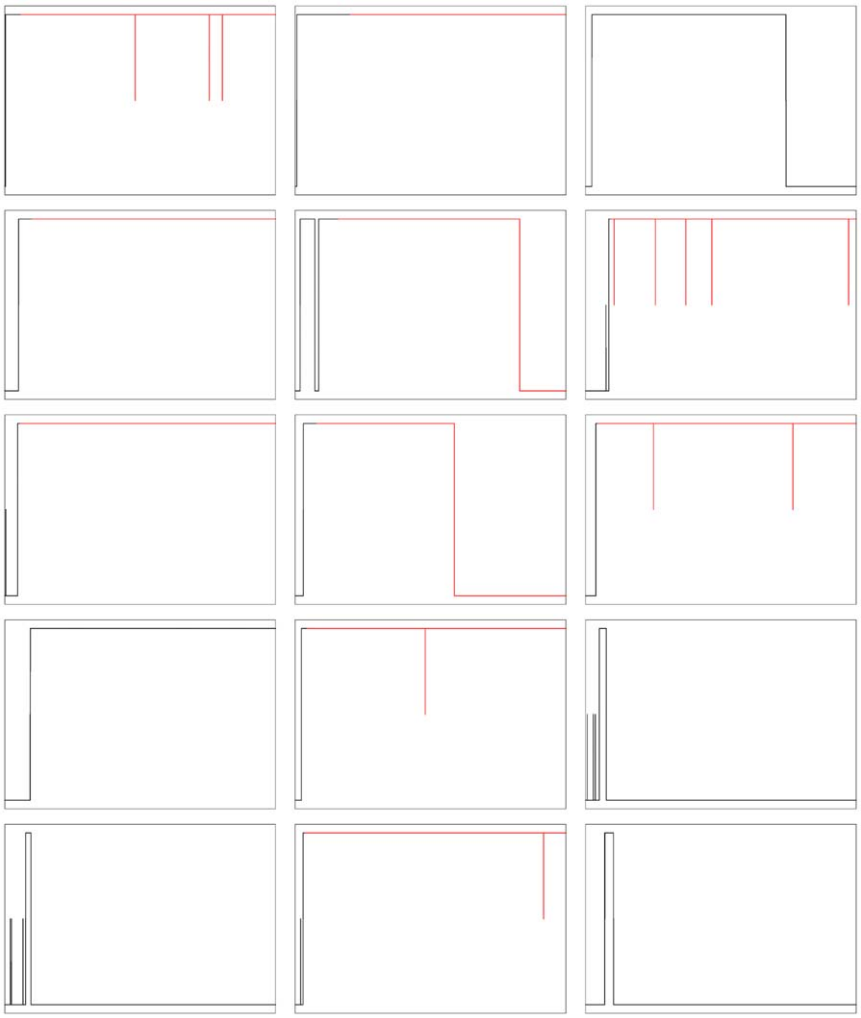

Figure 10. Calmodulin trapping on the level of single subunits. Each individual panel represents a single subunit chosen at random from the simulations from those subunits that bind calmodulin. The x-axis represents time, going from 0 to 300 s. The three levels in the y-dimension represent calmodulin binding, with no binding (lowest level), low-affinity binding (middle level) and high-affinity binding (highest level). Events of calmodulin sliding back and forth between the high-affinity and the low-affinity binding sites appear as drops from the top level to the centre and back up. The colour of the trace represents subunit phosphorylation at Thr286, with unphosphorylated subunits shown in black, and phosphorylated subunits in red.
doi:10.1371/journal.pone.0029406.g010

CaMKII. This suggests that at least one of the two conditions needs to be fulfilled in order for calmodulin trapping to happen: the existence of two binding sites or the compatibility of calmodulin binding and CaMKII inactivation.

Failure of a one-binding-site model to reproduce calmodulin trapping

The failure of the alternative one-binding site model to reproduce calmodulin trapping is perhaps not surprising: In the wildtype, the higher number of open subunits due to Thr286 autophosphorylation will increase the apparent k_{on} for calmodulin binding (since more binding sites will be available), but this has no influence on the apparent k_{off} after calcium withdrawal. Consider what happens to a calmodulin molecule bound to a CaMKII subunit in a one-binding-site scenario. Once calmodulin has dissociated from the only binding site, it is very quickly inactivated due to the lack of calcium, and is therefore no longer available to bind again. Importantly, this is independent of the autophosphorylation state of the subunit from which calmodulin has dissociated, so there is no difference in apparent k_{off} between wildtype and T286A autophosphorylation mutants. In order to reproduce trapping, a one-binding-site model would need to include an ad hoc increase in calmodulin affinity for autophosphorylated CaMKII, as has indeed been done in previous models of CaMKII activation (e.g. [24–27]). This will reproduce the effect, but without providing an explanation of the mechanism.

The full trapping model presented here overcomes the need for an ad hoc increase in affinity by postulating the existence of an additional binding site. In this case, not all of the calmodulin dissociating from the high-affinity site is immediately inactivated upon calcium withdrawal, but some of it merely "slides" to the low-affinity binding site and thus remains on the same subunit. In this case, autophosphorylation does matter: Phosphorylated subunits remain open and calmodulin can therefore "slide back" to the high-affinity binding site. In contrast, unphosphorylated subunits are likely to close, which makes re-binding to the high-affinity site impossible. The existence of a second binding site is thus important in order to retain calmodulin in the vicinity of the

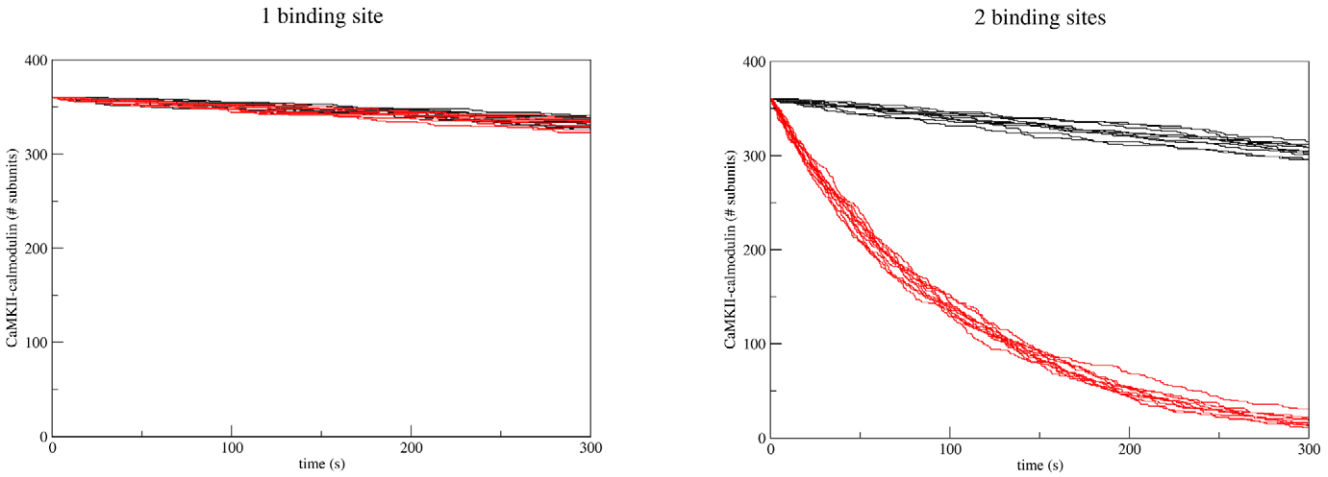

Figure 11. Comparison of the two-binding-site model with a one-binding site model. For each of the models, we ran ten simulations with wildtype CaMKII and ten simulations with the autophosphorylation deficient T286A mutant. All CaMKII molecules are open and fully saturated with calmodulin to begin with, and calmodulin is withdrawn, mimicking calcium withdrawal, at the start of the simulation. The ratio of calmodulin to CaMKII concentrations was the same as used in the experimental setup by Meyer et al. [18]. The number of calmodulin-bound monomeric CaMKII subunits is plotted against time. Wildtype is shown in black, T286A mutant in red. There is no difference in slope between mutant and wildtype in the one-binding-site model, whereas the two-binding-site model displays a clear difference between wildtype and mutant.
doi:10.1371/journal.pone.0029406.g011

high-affinity binding site for a while after it has dissociated, rather than releasing it completely.

By the same argument, binding to one of the binding sites has to be compatible with closing of the CaMKII subunit. Otherwise, a CaMKII subunit would only be able to close once calmodulin has completely dissociated from it, which means that the additional stabilisation of the open state by autophosphorylation at Thr286 has no effect on the apparent k_{off} (although, again, it would have an effect on apparent k_{on}). Thus, a two-binding-sites model where binding of calmodulin to one of the sites is compatible with the CaMKII subunit closing seems to be necessary for calmodulin trapping, unless some other yet unknown mechanism is involved.

It has been suggested that autophosphorylation at Thr286 could induce a conformational change which increases calmodulin affinity [28]. Interestingly, a key residue involved in this conformational change, residue Phe293 [28,32] is specific to high-affinity calmodulin binding in our model (see Figure 7). Our view is that phosphorylation at Thr286 stabilises a conformation conducive to calmodul in binding (rather than inducing such a conformation), but this interpretation is, as far as we can see, compatible with the structural data [28].

To summarise, the existence of two modes of calmodulin binding to CaMKII seems to be compatible with a wealth of existing experimental data. We show that this is both necessary and sufficient to explain calmodulin trapping and provide the first computational model in which calmodulin trapping arises as a feature of the entire system, rather than being hard coded as an explicit change in macroscopic parameters.

Binding of calmodulin to a closed structure of CaMKII

As described above, the trapping model proposed here requires calmodulin being able to bind to closed forms of CaMKII, a requirement which seems structurally plausible. This means that binding of calmodulin to CaMKII as such is not sufficient for CaMKII activation, although binding of calmodulin to the high-affinity site is. But the structural model goes even further than that: Not only does calmodulin binding to the low-affinity site seem compatible with closing, but it even seems to favour the closed conformation of CaMKII. This is because calmodulin, while bound to the inhibitory helix, also interacts with a lysine residue in the catalytic domain of CaMKII, thereby keeping those two domains in close proximity. This is a key prediction of our model, and one that has not been made elsewhere. Further investigations will be necessary to shed light on the detailed mechanism and functional role of such an interaction.

Detailed mechanism of calmodulin binding to CaMKII

Calmodulin has two calcium-binding lobes which are connected by a flexible helix. Both lobes are involved in binding CaMKII. We have previously published an allosteric model describing calcium binding to calmodulin and the calcium-dependent activation of CaMKII [36]. It has been suggested, however, that calmodulin binding to CaMKII is a sequential process where one lobe of calmodulin makes contact with CaMKII first, which then facilitates binding of the second lobe [37–39]. Such a mechanism would allow for a low-affinity binding mode (when only one lobe of calmodulin is bound to CaMKII) and a high-affinity binding mode (when both lobes are bound) to exist even in the absence of two calmodulin binding sites. This raises the possibility that what has been identified as a low-affinity and a high-affinity binding site in the experiments by [19] could actually just reflect partial vs full binding of calmodulin to CaMKII. However, the published structure of calmodulin binding to what corresponds to the low-affinity binding site on the CaMKII helix (PDB ID: 1CM1, chains A and B) [29] is one of fully bound calmodulin, suggesting that two calmodulin binding sites do indeed exist.

Our model has disregarded partial binding of calmodulin. The first reason for this is the design of our structural model, which was based on a starting structure of calmodulin fully bound to CaMKII (PDB ID: 1CM1, chains A and B) [29], i.e. where calmodulin "wraps around" its target. Our molecular dynamics simulations have not allowed for flexibility within the calmodulin molecule, thus preventing us from picking up hypothetical structures of calmodulin that is partly bound to CaMKII (and where, presumably, the conformation of the flexible helix connecting the two lobes would be quite different from the fully bound state).

Second, we consider partial binding of only the N- or the C-lobe of calmodulin to CaMKII as a transient initial state, which facilitates (and therefore very often results in) full binding of both lobes.

Our model includes calmodulin "sliding" back and forth between the low-affinity and the high-affinity binding sites. These reactions are short-hands for a process or a combination of processes which are not known in detail. For instance, it seems reasonable to assume that since both binding sites are in close proximity to each other, once a calmodulin molecule dissociates from one of the sites, this drastically increases the local calmodulin concentration around the other binding site, and thus the probability of binding there. Similar mechanisms have been well described for facilitated diffusion of proteins along a DNA strand [40]. It is also conceivable that there might be some form of conformational change of calmodulin bound to the low-affinity site, which would allow it to move along the helix and bind to the high-affinity site, as suggested by Tse et al. [19] or that a conformational change in the CaMKII inhibitory helix might be involve in the transition [28]. The two sliding reactions in our model are summaries of these (and possibly other) processes without including details about the exact mechanisms involved. As Figure 10 illustrates, calmodulin sliding is indeed an important mechanism in our simulations, by which a subunit can extend the lifetime of its calmodulin-bound state, and calmodulin can change back and forth between the low-affinity and the high-affinity site several times before dissociation completely.

Potential experimental validation

While the structure of calmodulin bound to the low-affinity binding site of CaMKII is known, the structure of calmodulin bound to the high-affinity binding site is a prediction from our model. The experimental determination of this structure - for instance as a complex of calmodulin with a longer fragment of the CaMKII autoinhibitory helix than in previous studies - could be used to validate this model.

The model of calmodulin trapping predicts that calmodulin binding is not per se sufficient for CaMKII activation. This is another prediction that could be tested experimentally. This could be done using monomeric T286A mutant CaMKII in order to separate the effect of calmodulin binding from that of autophosphorylation and other inter-subunit interactions. In that scenario, by quantifying both calmodulin binding and CaMKII activation, we predict that there would be a small portion of CaMKII molecules that are not active, even though bound to calmodulin. This portion could be increased by additionally disrupting calmodulin binding to the high-affinity (but not the low-affinity) binding site on CaMKII.

Conclusion

Calmodulin trapping upon CaMKII autophosphorylation might have an important role in synaptic plasticity by fine-tuning both CaMKII activity and calmodulin availability. We have combined structural modelling and stochastic simulations into a model that offers a detailed mechanistic explanation of calmodulin trapping. The model relies on two main ideas: First, the existence of two calmodulin binding sites on a given CaMKII subunit - an assumption backed by biochemical studies and our own structural work - and second, on the compatibility of calmodulin binding to one of these sites with CaMKII inactivity. Crucially, our model does not rely on any ad hoc assumptions about parameter changes after CaMKII autophosphorylation. Instead, the change in apparent k_{off} upon autophosphorylation, i.e. calmodulin trapping, is an emergent property that follows from the mechanisms of calmodulin binding and CaMKII conformational change. Our model thus offers a mechanistic explanation of calmodulin trapping, rather than just reproducing the effect. It provides a basis for further research in synaptic plasticity and memory, but possibly also in other fields where CaMKII signalling plays a role, including apoptosis (reviewed in [41,42]) and the cardiovascular system (reviewed in [43]).

Methods

Structure of a CaMKII subunit bound to calmodulin

Structural models were developed using the MODELLER software [44]. In order to obtain the structure of calmodulin-bound CaMKII, we used as templates previously published structures of the kinase domain of *C. elegans* CaMKII (PDB ID: 2BDW, chain A) [13] and of calmodulin bound to a fragment of the inhibitory helix of bovine CaMKII (PDB ID: 1CM1, chains A and B) [29]. The target sequence of calmodulin bound to the full kinase domain of CaMKII was created by combining the sequences of the two template PDB structures (chain A of 2BDW and chain A of 1CM1). The function automodel in MODELLER was used in order to model the unknown structure of the newly generated sequence, using the alignment file and the known structures of 2BDW and 1CM1 as inputs. The initial result featured two interlocking loops (residues 53–61 in the calmodulin structure and residues 159–163 in the kinase domain structure). In order to resolve this issue, loop refinement was performed using the Discrete Optimized Protein Energy (DOPE) method [45] with MODELLER. Out of 10 iterations, the structure with the minimal molpdf score (139.06694) was selected for further refinement using Amber 7 [46]. The ff94 force field was used and the molecule was solvated in a WATBOX216 water box with a 2.2 nm cutoff using tleap. We used Sander for energy minimisation (parameters used: imin = 1, maxcyc = 100, cut = 300.0, igb = 2, saltcon = 0.2, gbsa = 1, ntpr = 10, ntx = 1, ntb = 0). The result of the minimisation step was then used as an input for molecular dynamics using sander (parameters used: ntb = 0, ntt = 1, tautp = 0.5, dtemp = 2.0, nstlim = 5000, dt = 0.002, ntc = 2, ntf = 2, cut = 15, nsnb = 9999, ntpr = 20, ntwx = 20, all other parameters set to the default value).

Modelling CaMKII opening with a flexible helix

In order to model a potential open structure of CaMKII, the structure of the kinase domain (PDB ID: 2BDW, chain A) [13] was split into two parts: the autoinhibitory helix only and the rest of the kinase domain. Structural information about the four residues that link the two domains (Ser277 to His280 in the *C. elegans* sequence) was omitted. This was done in order to allow those residues to move freely in the course of the simulation, thereby allowing the autoinhibitory helix to move away from the kinase domain. Using the automodeller function of MODELLER, we iteratively generated 100 structures using those two partial structures as an input. The same two structures and the structure of calmodulin bound to a fragment of the inhibitory helix (PDB ID: 1CM1, chains A and B) were then used as templates for modelling the structure of calmodulin bound to the low-affinity site of a potentially open state of CaMKII. This was done using MODELLER and loop refinement was again performed using DOPE. Molecular dynamics was performed on the resulting structure using Amber 7: tleap was used for solvation using the ff94 force field and a WATBOX216 water box with a 4.0 nm cutoff. Sander was used for minimisation (parameters as above) and molecular dynamics (parameters as above).

Structure of calmodulin bound to the high-affinity site

The fragment containing the high-affinity binding site used by Tse et al. [19] is seven residues longer than the fragment

containing the low-affinity binding site. We assumed the high-affinity binding site to be towards the middle of these seven residues, i.e. one turn further towards the inside of the CaMKII inhibitory helix than the low-affinity binding site. Therefore the structure of CaMKII bound to the low-affinity site used before (PDB ID: 1CM1, chains A and B) was modified by manually translating the inhibitory helix by one turn in PyMOL (http://www.pymol.org). Note that this assumption was merely used to find a starting point for simulations away from the established low-affinity binding site. The identification of the precise residues that contribute to the interaction was left to the molecular dynamics simulations. Together with the structure of the kinase domain (PDB ID: 2BDW, chain A), this was then used to create a putative combined structure using the automodel function in MODELLER, as described above. Again, tleap in Amber 7 was used for solvation, this time with a larger solvent box (4.0 nm). Energy minimisation and molecular dynamics were performed using sander (parameters as described above). Binding of calmodulin to the high-affinity site of a potentially open structure was modelled using separate structures for the inhibitory helix and the rest of the kinase domain, as described above. MODELLER was used to generate an initial structure, which was used as an input for Amber 7: The structure was solvated using tleap (with a 5.0 nm water box), and sander was used to run both minimisation and molecular dynamics (parameters as above).

All figures of protein structures in this paper were created using PyMOL [47].

Kinetics of calmodulin binding to the high-affinity binding site

For biochemical modelling, we needed to determine parameters describing calmodulin binding to the low-affinity binding site of CaMKII, calmodulin binding to the high-affinity binding site and "sliding" of calmodulin from the high-affinity to the low-affinity binding site and back. These latter reactions describe an unknown underlying mechanism (or collection of mechanisms) by which binding of a calmodulin molecule to one of the two binding sites might facilitate subsequent binding to the other binding site on the same CaMKII subunit.

The affinity of calmodulin for the low-affinity binding site was 5.9×10^{-6} M, corresponding to the low-affinity peptide used by Tse et al. [19]. Meyer et al. have reported a forward rate of 0.5×10^{8} M-1·s-1 for calmodulin binding to a phosphorylated CaMKII dodecamer [18]. To compute a microscopic forward rate for an individual subunit, we divided this number by 12 (the number of subunits that make up a holoenzyme) and obtained a rate of 4.2×10^{6} M-1·s-1. This is close to the value of 3.2×10^{6} M-1·s-1 reported by Tzortzopoulos and Török [48].

Just like the short fragment used by Tse et al. [19] corresponds to the low-affinity binding site, we took the long fragment (291–312) to correspond to the high-affinity binding site. This is also backed up by earlier findings that have implied residues contained in the longer fragment in high-affinity binding, notably residues 293–295 and residues 296–298 [33]. It has also been observed that binding of calmodulin to a similar fragment (residues 290–314) mimicked calmodulin binding to the entire phosphorylated kinase, suggesting that the entire high-affinity binding domain is indeed contained in this fragment [49]. Since access to the binding site is more constrained in the context of an entire holoenzyme (compared to a relatively short fragment), we expect the in vivo K_d for high-affinity binding of calmodulin to be higher than that. The K_d of the long fragment thus provides a lower limit. This K_d is given by Tse et al. as 7×10^{-14} M [19], but Waxham et al. report a K_d of 2×10^{-13} M for the same fragment [33].

Meyer et al. [18] report a K_d of 6×10^{-11} for calmodulin binding to autonomous CaMKII. In our model, autonomous CaMKII will not display subunit opening or closing, so the apparent calmodulin dissociation constant is only a function of the microscopic low-affinity and high-affinity dissociation constants. Since the dissociation constant of the low-affinity binding site, as reported above, is several orders of magnitude bigger than the combined dissociation constant, we concluded that the low-affinity binding site contributes very little to the overall affinity of the fragment and that the low overall K_d is due almost entirely to the high-affinity binding site. We therefore set the microscopic K_d for the high-affinity binding site to 6×10^{-11} M. This is indeed higher than the K_d values reported elsewhere for the long fragment [19,33].

In terms of Gibbs free energies, the K_d for high-affinity binding we chose corresponds to a (standardised) ΔG of -5.9×10^{-4} J/mol, and the K_d for low-affinity binding to a ΔG of -3.0×10^{-4} J/mol. Although the number of - partly hidden - assumptions underlying energy calculation makes it difficult to directly compare these values with the energies reported for the protein complex in the molecular dynamics simulations, in both cases the ratio between the high-affinity and the low-affinity energy is similar.

We assumed that "sliding" of calmodulin from the low-affinity site to the high-affinity site is intrinsically symmetrical, i. e. that once dissociated from one binding site, the probability of binding to the other binding site should be the same in either direction. Therefore, the equilibrium constant for the sliding reaction (and hence, the probability of sliding from one site to the other) should be determined by the dissociation rates (and hence, the dissociation constants) for both sites:

$$K_{sliding}=\frac{K_{d_{ha}}}{K_{d_{la}}} \tag{1}$$

Using this equation, we concluded that calmodulin bound to the low-affinity site will "slide" to the high-affinity binding site with a probability of 0.99999.

Subunit opening and closing

In order to obtain an estimate of the opening probability of a single CaMKII subunit, we used COPASI [50] and constructed a model of calmodulin binding to a single CaMKII subunit which could open or close based on the above parameters. The model contains only ten reactions, six of which describe binding and dissociation of calmodulin to the two binding sites on an unoccupied CaMKII subunit (in the open state for the high-affinity binding site, in both the open and the closed state for the low-affinity binding site), two describe "sliding" of calmodulin between the two binding sites and two describe opening and closing of the CaMKII subunit. The full list of reactions is given in Table S1.

The calmodulin concentration used in this model was 10^{-5} M and the concentration of CaMKII peptide was 10^{-4} M, corresponding to the experimental concentrations used by Tse et al. [19]. We started the simulations with all of the peptide in the unbound state.

This model was used to optimise the probability of CaMKII opening. As an objective function, we used the apparent combined K_d for a single subunit:

Table 2. List of parameters for the model of calmodulin trapping.

Parameter	value	reference
k_f for CaMKII phosphorylation at residue 286	$30 s^{-1}$	[55]
k_f for dephosphorylation of CaMKII at residue 286 by PP1	$1.6\times10^{-7} s^{-1}$	computed from [56]
k_f for CaMKII phosphorylation at residue 306	$0.55 s^{-1}$	[55]
k_f for dephosphorylation of CaMKII at residue 306 by PP1	$1.6\times10^{-7} s^{-1}$	computed from [56]
K_d for calmodulin binding to the low-affinity site of CaMKII	$5.9\times10^{-6} M$	[19]
k_f for calmodulin binding to the low-affinity site of CaMKII	$4.2\times10^{6} M^{-1}s^{-1}$	[18]
k_b for calmodulin binding to the low-affinity site of CaMKII	$24.8 s^{-1}$	$K_d \times k_f$
K_d for calmodulin binding to the high-affinity site of CaMKII	$6\times10^{-11} M$	*this study*
k_f for calmodulin binding to the high-affinity site of CaMKII	$4.2\times10^{6} M^{-1}s^{-1}$	[18]
k_b for calmodulin binding to the high-affinity site of CaMKII	$2.5\times10^{-4} s^{-1}$	$K_d \times k_f$
probability of spontaneous CaMKII opening	0.002	*this study*
probability of calmodulin sliding to the high-affinity site	0.99999	*this study*
total number of CaMKII subunits used for simulation	360	total number of CaMKII subunits in the PSD [52]
total number of calmodulin molecules used for simulation	450	*this study*
reaction volume used for simulation	$5\times10^{-14} l$	*this study*

List of parameters for the model of calmodulin trapping.
doi:10.1371/journal.pone.0029406.t002

$$K_{d_{combined}} = \frac{([open]+[closed])[CaM]}{[closed-CaM]_{la}+[open-CaM]_{la}+[open-CaM]_{ha}} \quad (2)$$

This value has been reported by Tzortzopoulos and Török [48] to be $4\times10^{-8} M$ for calmodulin binding to CaMKII with a T286A mutation. This was chosen in order to isolate the effects of calmodulin binding and opening/closing only, without having to account for autophosphorylation. The *Genetic Algorithm SR* optimisation function in COPASI [50] was run ten times, with ten randomly chosen initial values. We used the default settings for the *Genetic Algorithm SR* function (200 generations, a population size of 20 and random number generator 1, all other values set to zero). The resulting value for the opening probability was 0.002.

All other parameters were taken from the literature. A full list is given in table 2.

Stochastic simulations

Stochastic simulations were performed using StochSim [51]. The total duration of the simulation was 300 s.The software was allowed to optimise the time increment, with data being read out every millisecond. We used a total of 360 CaMKII subunits, corresponding to the number of CaMKII subunits typically found in a postsynaptic density [52], in order to facilitate future simulations under physiological conditions. Both the number of calmodulin molecules (450) and the total reaction volume ($5\times10^{-14} l$) were chosen to preserve the concentrations and CaMKII-to-calmodulin ratio used in the experiments performed by Meyer et al. [18].

For the two-binding-site wildtype model, all CaMKII subunits were closed, unphosphorylated and not bound to calmodulin at the outset of the simulation. Calmodulin was present at the beginning, but removed after 30 s to mimic calcium withdrawal. The complete StochSim input files for this model are given in Dataset S3. The T286A mutation was implemented by setting the Thr286 autophosphorylation rate to zero in a model otherwise identical to that for the wildtype.

The one-binding-site model was the same as the two-binding-site model, except that the reaction describing calmodulin binding to the low-affinity site and the rapid equilibrium governing calmodulin "sliding" from the low-affinity to the high-affinity site were removed. Everything else (including the definition of the state flags) was kept as it was. In the one-binding site scenario, Thr286 phosphorylation also had a marked effect on the apparent on rate of calmodulin binding. In order to separate this effect from the actual trapping effect (the change in off rate), the initial calmodulin binding phase was not explicitly modelled. Instead, all 360 CaMKII subunits were open, calmodulin-bound and (for wildtype CaMKII) phosphorylated at Thr286 at the outset of the simulation, and calmodulin was withdrawn from the beginning of the simulation. Simulations were run for 300 s, with an automatically optimised time step, as above. Again, the T286A mutant differed from the wildtype by the Thr286 autophosphorylation rate being set to zero.

To allow for direct comparison between the two-binding-site and one-binding-site models, simulations of the two-binding-site models were run under the same conditions as for the one-binding-site model, i. e. with all CaMKII calmodulin-bound at the outset and calmodulin withdrawn at the beginning of the simulation.

Ten StochSim simulation runs were performed for each of the models. All simulations were run on a Centos 5.4 Linux LSF Cluster containing 350 nodes with 32GB RAM or more each. The longest simulations took a few hours to complete.

Supporting Information

Table S1 We used a simple model of a single CaMKII subunit which could open, close and bind to calmodulin to determine the opening probability of CaMKII using the parameter search facility of COPASI [50]. The full list of reactions of this model is given in this table.
(PDF)

Dataset S1 Structural model of calmodulin binding to the low-affinity binding site on a closed subunit of CaMKII.
(TXT)

Dataset S2 Structural model of calmodulin binding to the high-affinity binding site on a CaMKII subunit. When the inhibitory helix of CaMKII is allowed some flexibility, it moves away from the catalytic domain to accommodate for calmodulin binding to the high-affinity binding site. This exposes the catalytic site and the Thr286 autophosphorylation site.
(TXT)

Dataset S3 This dataset is a text file containing the input files for simulation with StochSim. Different parts of the model and the simulation are defined in section that must be copied to different files, as follows: STCHSTC.INI: Controls the parameters of the simulation, such as the time interval, the total simulation duration and the names of input and output files. MESSAGE.INI: List of StochSim error messages for trouble-shooting should the simulation exit. COMPLEX.INI: Contains information about the different components of the model and their initial concentrations. REACTION.INI: Contains all reactions, specifying substrates, products, and forward and backward reaction rates. MS_1.INI: Contains information pertaining to the state flags of CaMKII and to how these are affected by reactions and rapid equilibria. NS_1.INI Contains information about neighbour-sensitive reactions (in this case, only Thr286 phosphorylation). ARRAY.INI: Defines the geometry and composition of arrays (in this case, 60 hexamers of CaMKII). DYNAMIC.INI: Contains information about parameter values that change over time, used here to set the concentration of active calmodulin to zero after 30 seconds.
(TXT)

Author Contributions

Conceived and designed the experiments: MIS NL. Performed the experiments: MIS DPM. Analyzed the data: MIS. Contributed reagents/materials/analysis tools: MIS. Wrote the paper: MIS NL.

References

1. Bennett MK, Erondu NE, Kennedy MB (1983) Purification and characterization of a calmodulindependent protein kinase that is highly concentrated in brain. J Biol Chem 258: 12735–12744.
2. Silva AJ, Paylor R, Wehner JM, Tonegawa S (1992) Impaired spatial learning in alpha-calciumcalmodulin kinase II mutant mice. Science 257: 206–211.
3. Silva AJ, Stevens CF, Tonegawa S, Wang Y (1992) Deficient hippocampal long-term potentiation in alpha-calcium-calmodulin kinase II mutant mice. Science 257: 201–206.
4. Bliss TV, Lømo T (1973) Long-lasting potentiation of synaptic transmission in the dentate area of the anaesthetized rabbit following stimulation of the perforant path. J Physiol 232: 331–356.
5. Whitlock JR, Heynen AJ, Shuler MG, Bear MF (2006) Learning induces long-term potentiation in the hippocampus. Science 313: 1093–1097.
6. Mayer ML, Westbrook GL (1985) The action of N-methyl-D-aspartic acid on mouse spinal neurones in culture. J Physiol 361: 65–90.
7. Mayer ML, Westbrook GL (1987) Permeation and block of N-methyl-D-aspartic acid receptor channels by divalent cations in mouse cultured central neurones. J Physiol 394: 501–527.
8. Lisman J, Schulman H, Cline H (2002) The molecular basis of CaMKII function in synaptic and behavioural memory. Nat Rev Neurosci 3: 175–190.
9. Schulman H, Greengard P (1978) Ca2+-dependent protein phosphorylation system in membranes from various tissues, and its activation by "calcium-dependent regulator". Proc Natl Acad Sci USA 75: 5432–5436.
10. Schulman H, Greengard P (1978) Stimulation of brain membrane protein phosphorylation by calcium and an endogenous heat-stable protein. Nature 271: 478–479.
11. Lee HK, Barbarosie M, Kameyama K, Bear MF, Huganir RL (2000) Regulation of distinct AMPA receptor phosphorylation sites during bidirectional synaptic plasticity. Nature 405: 955–959.
12. Hayashi Y, Shi SH, Esteban JA, Piccini A, Poncer JC, et al. (2000) Driving AMPA receptors into synapses by LTP and CaMKII: requirement for GluR1 and PDZ domain interaction. Science 287: 2262–2267.
13. Rosenberg OS, Deindl S, Sung RJ, Nairn AC, Kuriyan J (2005) Structure of the autoinhibited kinase domain of CaMKII and SAXS analysis of the holoenzyme. Cell 123: 849–860.
14. Kolodziej SJ, Hudmon A, Waxham MN, Stoops JK (2000) Three-dimensional reconstructions of calcium/calmodulin-dependent (CaM) kinase II alpha and truncated CaM kinase II alpha reveal a unique organization for its structural core and functional domains. J Biol Chem 275: 14354–14359.
15. Hanley RM, Means AR, Kemp BE, Shenolikar S (1988) Mapping of calmodulin-binding domain of Ca2+/calmodulin-dependent protein kinase II from rat brain. Biochem Biophys Res Commun 152: 122–128.
16. Payne ME, Fong YL, Ono T, Colbran RJ, Kemp BE, et al. (1988) Calcium/calmodulin-dependent protein kinase II. Characterization of distinct calmodulin binding and inhibitory domains. J Biol Chem 263: 7190–7195.
17. Hanson PI, Meyer T, Stryer L, Schulman H (1994) Dual role of calmodulin in autophosphorylation of multifunctional CaM kinase may underlie decoding of calcium signals. Neuron 12: 943–956.
18. Meyer T, Hanson PI, Stryer L, Schulman H (1992) Calmodulin trapping by calcium-calmodulindependent protein kinase. Science 256: 1199–1202.
19. Tse JKY, Giannetti AM, Bradshaw JM (2007) Thermodynamics of calmodulin trapping by Ca2+/calmodulin-dependent protein kinase II: subpicomolar Kd determined using competition titration calorimetry. Biochemistry 46: 4017–4027.
20. Dosemeci A, Albers RW (1996) A mechanism for synaptic frequency detection through autophosphorylation of CaM kinase II. Biophys J 70: 2493–2501.
21. Zhabotinsky AM (2000) Bistability in the Ca(2+)/calmodulin-dependent protein kinasephosphatase system. Biophys J 79: 2211–2221.
22. Lisman JE, Zhabotinsky AM (2001) A model of synaptic memory: a CaMKII/PP1 switch that potentiates transmission by organizing an AMPA receptor anchoring assembly. Neuron 31: 191–201.
23. Miller P, Zhabotinsky AM, Lisman JE, Wang XJ (2005) The stability of a stochastic camkii switch: dependence on the number of enzyme molecules and protein turnover. PLoS Biol 3: e107.
24. Holmes WR (2000) Models of calmodulin trapping and CaM kinase II activation in a dendritic spine. J Comput Neurosci 8: 65–85.
25. Okamoto H, Ichikawa K (2000) A model for molecular mechanisms of synaptic competition for a finite resource. BioSystems 55: 65–71.
26. Kubota Y, Bower JM (2001) Transient versus asymptotic dynamics of CaM kinase II: possible roles of phosphatase. J Comput Neurosci 11: 263–279.
27. Zeng SY, Holmes WR (2010) The effect of noise on CaMKII activation in a dendritic spine during LTP induction. J Neurophysiol 103: 1798–1808.
28. Hoffman L, Stein RA, Colbran RJ, Mchaourab HS (2011) Conformational changes underlying calcium/calmodulin-dependent protein kinase II activation. EMBO J 30: 1251–1262.
29. Wall ME, Clarage JB, Phillips GN (1997) Motions of calmodulin characterized using both Bragg and diffuse X-ray scattering. Structure 5: 1599–1612.
30. de Diego I, Kuper J, Bakalova N, Kursula P, Wilmanns M (2010) Molecular basis of the deathassociated protein kinase-calcium/calmodulin regulator complex. Sci Signal 3: ra6.
31. Rellos P, Pike ACW, Niesen FH, Salah E, Lee WH, et al. (2010) Structure of the CaMKIIdelta/Calmodulin Complex Reveals the Molecular Mechanism of CaMKII Kinase Activation. PLoS Biol 8: e1000426.
32. Singla SI, Hudmon A, Goldberg JM, Smith JL, Schulman H (2001) Molecular characterization of calmodulin trapping by calcium/calmodulin-dependent protein kinase II. J Biol Chem 276: 29353–29360.
33. Waxham MN, Tsai AL, Putkey JA (1998) A mechanism for calmodulin (CaM) trapping by CaMkinase II defined by a family of CaM-binding peptides. J Biol Chem 273: 17579–17584.
34. Chin D, Means AR (2002) Mechanisms for regulation of calmodulin kinase IIalpha by Ca(2+)/calmodulin and autophosphorylation of threonine 286. Biochemistry 41: 14001–14009.
35. Yamauchi T (2005) Neuronal Ca2+/calmodulin-dependent protein kinase II–discovery, progress in a quarter of a century, and perspective: implication for learning and memory. Biol Pharm Bull 28: 1342–1354.
36. Stefan MI, Edelstein SJ, Le Novére N (2008) An allosteric model of calmodulin explains differential activation of PP2B and CaMKII. Proc Natl Acad Sci USA 105: 10768–10773.
37. Byrne MJ, Putkey JA, Waxham MN, Kubota Y (2009) Dissecting cooperative calmodulin binding to CaM kinase II: a detailed stochastic model. J Comput Neurosci 27: 621–638.
38. Jama AM, Fenton J, Robertson SD, Trk K (2009) Time-dependent autoinactivation of phospho-Thr286-alphaCa2+/calmodulin-dependent protein kinase II. J Biol Chem 284: 28146–28155.
39. Pepke S, Kinzer-Ursem T, Mihalas S, Kennedy MB (2010) A dynamic model of interactions of Ca2+, calmodulin, and catalytic subunits of Ca2+/calmodulin-dependent protein kinase II. PLoS Comput Biol 6: e1000675.

40. Berg OG, Winter RB, von Hippel PH (1981) Diffusion-driven mechanisms of protein translocation on nucleic acids. 1. Models and theory. Biochemistry 20: 6929–6948.
41. Cohen MB, Rokhlin OW (2009) Mechanisms of prostate cancer cell survival after inhibition of AR expression. J Cell Biochem 106: 363–371.
42. Brnjic S, Olofsson MH, Havelka AM, Linder S (2010) Chemical biology suggests a role for calcium signaling in mediating sustained JNK activation during apoptosis. Mol Biosyst 6: 767–774.
43. Bers DM, Grandi E (2009) Calcium/calmodulin-dependent kinase II regulation of cardiac ion channels. J Cardiovasc Pharmacol 54: 180–187.
44. Šali A, Blundell TL (1993) Comparative protein modelling by satisfaction of spatial restraints. J Mol Biol 234: 779–815.
45. Shen MY, Sali A (2006) Statistical potential for assessment and prediction of protein structures. Protein Sci 15: 2507–2524.
46. Case D, Pearlman D, Caldwell J, Cheatham III T, Wang J, et al. (2002) AMBER 7. University of California, San Francisco.
47. DeLano Scientific LLC (2009) The PyMOL molecular graphics system, version 1.2r1.
48. Tzortzopoulos A, Török K (2004) Mechanism of the T286A-mutant alphaCaMKII interactions with Ca2+/calmodulin and ATP. Biochemistry 43: 6404–6414.
49. Putkey JA, Waxham MN (1996) A peptide model for calmodulin trapping by calcium/calmodulindependent protein kinase II. J Biol Chem 271: 29619–29623.
50. Hoops S, Sahle S, Gauges R, Lee C, Pahle J, et al. (2006) COPASI–a COmplex PAthway SImulator. Bioinformatics 22: 3067–3074.
51. Le Novére N, Shimizu TS (2001) STOCHSIM: modelling of stochastic biomolecular processes. Bioinformatics 17: 575–576.
52. Petersen JD, Chen X, Vinade L, Dosemeci A, Lisman JE, et al. (2003) Distribution of postsynaptic density (PSD)-95 and Ca2+/calmodulin-dependent protein kinase II at the PSD. J Neurosci 23: 11270–11278.
53. Pettersen EF, Goddard TD, Huang CC, Couch GS, Greenblatt DM, et al. (2004) UCSF Chimera–a visualization system for exploratory research and analysis. J Comput Chem 25: 1605–1612.
54. Le Novére N, Hucka M, Mi H, Moodie S, Schreiber F, et al. (2009) The Systems Biology Graphical Notation. Nat Biotechnol 27: 735–741.
55. Lučić V, Greif G, Kennedy M (2008) Detailed state model of CaMKII activation and autophosphorylation. Eur Biophys J 38: 83–98.
56. Strack S, Barban MA, Wadzinski BE, Colbran RJ (1997) Differential inactivation of postsynaptic density-associated and soluble Ca2+/calmodulin-dependent protein kinase II by protein phosphatases 1 and 2A. J Neurochem 68: 2119–2128.